J. Fluid Mech. (2016), *vol.* 805, *pp.* 322–354. © Cambridge University Press 2016
doi:10.1017/jfm.2016.567

Marangoni waves in two-layer films under the action of spatial temperature modulation

Alexander A. Nepomnyashchy[1,2] **and Ilya B. Simanovskii**[1,†]

[1]Department of Mathematics, Technion – Israel Institute of Technology, 32000, Haifa, Israel

[2]Minerva Center for Nonlinear Physics of Complex Systems, Technion – Israel Institute of Technology, 32000, Haifa, Israel

(Received 10 February 2016; revised 12 July 2016; accepted 23 August 2016;
first published online 20 September 2016)

The nonlinear dynamics of waves generated by the deformational oscillatory Marangoni instability in a two-layer film under the action of a spatial temperature modulation on the solid substrate is considered. A system of long-wave equations governing the deformations of the upper surface and the interface between the liquids is derived. The nonlinear simulations reveal the existence of numerous dynamical regimes, including two-dimensional stationary flows and standing waves, three-dimensional standing waves with different spatial periods, and three-dimensional travelling waves. The general diagram of the flow regimes is constructed.

Key words: instability, interfacial flows (free surface), thin films

1. Introduction

During recent decades, a great deal of attention has been paid to the investigation of nonlinear patterns created by instabilities (Cross & Hohenberg 1993). The nonlinear dynamics of systems subjected to oscillatory instabilities is especially rich (Aranson & Kramer 2002). For nonlinear patterns, a multistability is characteristic; specifically, in spatially extended systems different pattern planforms are possible.

An important problem is to control the development of instability, i.e. the suppression of undesired kinds of patterns or generation of desired kinds of patterns (Mikhailov & Showalter 2006; Schöll & Schuster 2008).

A possible way of controlling the pattern selection is a spatial modulation of the control parameter. It is necessary to distinguish between patterns created by short-wave instabilities, characterized by a non-zero critical wavenumber $k_c \neq 0$, and patterns generated by long-wave instabilities, where the critical wavenumber $k_c = 0$, so that the wavenumber interval of instability is $0 < k < k_m$. The influence of the spatial modulation of the control parameter on short-wave patterns with moduli of wavevectors close to k_c is rather well understood. The action of a resonant spatially periodic forcing on the onset of stationary patterns created by a short-wave instability has been explored extensively (Vozovoi and Nepomnyashchy 1974; Vozovoi & Nepomnyashchy 1979; Coullet, Elphick & Repaux 1987; Pismen 1987; Manor, Hagberg & Meron 2008; Freund, Pesch & Zimmermann 2011; Mau *et al.* 2013; Haim, Mau & Meron 2014; Weiss, Seiden & Bodenschatz 2014). The influence of resonant and non-resonant spatial modulations on short-wave oscillatory

† Email address for correspondence: yuri11@inter.net.il

instabilities was studied on the background of a complex Ginzburg–Landau equation by Nepomnyashchy (1988), Malomed (1993), Utzny, Zimmermann & Bär (2002), Hammele & Zimmermann (2006), Abarzhi *et al.* (2007) and Nepomnyashchy & Abarzhi (2010).

In the case of a long-wave instability, where disturbances with significantly different wavenumbers are relevant, the prediction of the pattern dynamics is much more difficult. In the absence of a control, the pattern evolution is governed by the nonlinear interaction of disturbances with different wavevectors, which can lead to complex spatio-temporal dynamics. It is tempting to impose a spatial modulation of the control parameter with a prescribed wavelength, which can simplify the dynamics and make it more predictable. However, the effect of the spatial modulation on long-wave patterns has still hardly been explored.

This paper is devoted to the investigation of an important class of long-wave oscillatory instabilities which cannot be described by the Ginzburg–Landau equation (Nepomnyashchy & Shklyaev 2016). This kind of instability is typical for liquid systems with deformable interfaces. To the best of our knowledge, the influence of spatial modulations on long-wave oscillatory instabilities has never been studied before.

We consider the nonlinear dynamics of waves generated by the deformational Marangoni instability in a two-layer film under the action of a spatial temperature modulation on the solid substrate. In the absence of a temperature modulation, a two-layer film is subject to a long-wave oscillatory instability by heating from above (Nepomnyashchy & Simanovskii 2007). In contradistinction to a one-layer film, where the deformational instability is monotonic and leads to film rupture, an oscillatory instability in a two-layer film creates various wavy patterns (Nepomnyashchy & Simanovskii 2007, 2012). The formulation of the problem is given in § 2. In § 3, we derive a system of long-wave equations that govern the evolution of the surface deformations. The results of nonlinear simulations are presented in § 4. Section 5 contains concluding remarks.

2. Formulation of the problem

Consider a system of two superposed layers of immiscible liquids with different physical properties (see figure 1). The bottom layer rests on a solid substrate and the top layer is in contact with the adjacent gas phase. The temperature of the solid substrate is $T_s(x, y)$ (we assume that T_s is a slow function of x and y), and the temperature of the gas is T_g. All of the variables referring to the bottom layer are marked by a subscript 1 and all of the variables referring to the top layer are marked by a subscript 2. The coordinates of the interfaces in a quiescent state are $z = H_m^0$, $m = 1, 2$. The deformable interfaces are described by the equations $z = H_1(x, y, t)$ (liquid–liquid interface) and $z = H_2(x, y, t)$ (liquid–gas interface). The mth fluid has density ρ_m, kinematic viscosity ν_m, dynamic viscosity $\eta_m = \rho_m \nu_m$, thermal diffusivity χ_m and heat conductivity κ_m. The surface tension coefficients on the lower and upper interfaces, σ_1 and σ_2, are linear functions of temperature T: $\sigma_1 = \sigma_1^0 - \alpha_1 T$, $\sigma_2 = \sigma_2^0 - \alpha_2 T$. We do not consider the effect of gravity, which is negligible for sufficiently thin layers.

The complete system of nonlinear equations governing Marangoni convection is written in the following form (Simanovskii & Nepomnyashchy 1993):

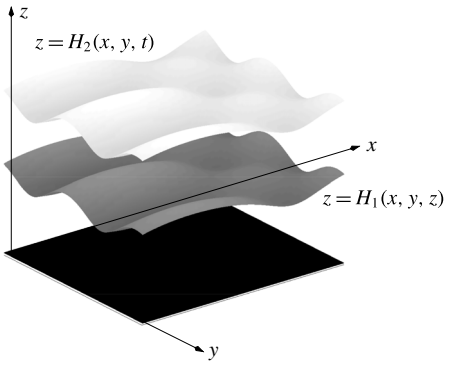

FIGURE 1. Geometric configuration of the region and coordinate axes.

$$\frac{\partial \boldsymbol{v}_m}{\partial t} + (\boldsymbol{v}_m \cdot \nabla)\boldsymbol{v}_m = -\frac{1}{\rho_m}\nabla p_m + \nu_m \Delta \boldsymbol{v}_m, \tag{2.1}$$

$$\frac{\partial T_m}{\partial t} + \boldsymbol{v}_m \cdot \nabla T_m = \chi_m \Delta T_m, \tag{2.2}$$

$$\nabla \cdot \boldsymbol{v}_m = 0, \quad m = 1, 2. \tag{2.3}$$

Here, $\boldsymbol{v}_m$ and p_m are the velocity and the difference between the overall pressure and the atmospheric pressure in the mth liquid respectively. The boundary conditions on the rigid boundary are

$$\boldsymbol{v}_1 = 0, \quad T_1 = T_s(x, y); \quad \text{at } z = 0. \tag{2.4a,b}$$

On the deformable interface $z = H_1$, the following boundary conditions hold: the balance of normal stresses,

$$p_2 - p_1 + 2\sigma_1 K_1 = \left[-\eta_1\left(\frac{\partial v_{1i}}{\partial x_k} + \frac{\partial v_{1k}}{\partial x_i}\right) + \eta_2\left(\frac{\partial v_{2i}}{\partial x_k} + \frac{\partial v_{2k}}{\partial x_i}\right)\right] n_{1i} n_{1k}; \quad i, k = 1, 2, 3; \tag{2.5}$$

the balance of tangential stresses,

$$\left[-\eta_1\left(\frac{\partial v_{1i}}{\partial x_k} + \frac{\partial v_{1k}}{\partial x_i}\right) + \eta_2\left(\frac{\partial v_{2i}}{\partial x_k} + \frac{\partial v_{2k}}{\partial x_i}\right)\right] \tau_{1i}^{(l)} n_{1k} - \alpha_1 \tau_{1i}^{(l)} \frac{\partial T_1}{\partial x_i} = 0; \quad l = 1, 2; \; i, k = 1, 2, 3; \tag{2.6}$$

the continuity of the velocity field,

$$\boldsymbol{v}_1 = \boldsymbol{v}_2; \tag{2.7}$$

the kinematic equation for the interface motion,

$$\frac{\partial H_1}{\partial t} + v_{1x}\frac{\partial H_1}{\partial x} + v_{1y}\frac{\partial H_1}{\partial y} = v_{1z}; \tag{2.8}$$

the continuity of the temperature field,

$$T_1 = T_2; \tag{2.9}$$

and the balance of normal heat fluxes,

$$\left(\kappa_1 \frac{\partial T_1}{\partial x_i} - \kappa_2 \frac{\partial T_2}{\partial x_i}\right) n_{1i} = 0. \tag{2.10}$$

Similar boundary conditions are imposed on the deformable interface $z = H_2$:

$$-p_2 + 2\sigma_2 K_2 = -\eta_2 \left(\frac{\partial v_{2i}}{\partial x_k} + \frac{\partial v_{2k}}{\partial x_i}\right) n_{2i} n_{2k}, \tag{2.11}$$

$$-\eta_2 \left(\frac{\partial v_{2i}}{\partial x_k} + \frac{\partial v_{2k}}{\partial x_i}\right) \tau_{2i}^{(l)} n_{2k} - \alpha_2 \tau_{2i}^{(l)} \frac{\partial T_3}{\partial x_i} = 0, \quad l = 1, 2, \; i, k = 1, 2, 3, \tag{2.12}$$

$$\frac{\partial H_2}{\partial t} + v_{2x} \frac{\partial H_2}{\partial x} + v_{2y} \frac{\partial H_2}{\partial y} = v_{2z}. \tag{2.13}$$

In the formulae presented above, K_1 and K_2 are the mean curvatures, $\boldsymbol{n}_1$ and $\boldsymbol{n}_2$ are the normal vectors and $\boldsymbol{\tau}_1^{(l)}$ and $\boldsymbol{\tau}_2^{(l)}$ are the tangential vectors of the lower and upper interfaces. In the quantities with two subscripts, the first subscript corresponds to the number of the liquid ($m = 1, 2$) and the second subscript determines the number of the Cartesian coordinate ($i, k = 1, 2, 3$; $x_1 = x$, $x_2 = y$, $x_3 = z$). The usual summation convention is applied. For a heat flux on the liquid–gas interface we use an empirical condition,

$$\kappa_2 \frac{\partial T_2}{\partial x_i} n_{2i} = -q(T_2 - T_g), \tag{2.14}$$

where q is the heat exchange coefficient, which is assumed to be constant.

3. Derivation of the long-wave amplitude equations

The system of equations and boundary conditions (2.1)–(2.14) is rather complicated. However, in this paper we will consider the case where the characteristic spatial scale of the temperature modulation of the substrate is much larger than the thickness of the layer, i.e. the temperature modulation depends on the scaled coordinates $\tilde{X} = \epsilon x$ and $\tilde{Y} = \epsilon y$, $\epsilon \ll 1$, rather than on x and y. Later on, we assume that the solution of the equations and boundary conditions (2.1)–(2.14) itself depends only on the slow variables, $\tilde{\boldsymbol{X}} = (\tilde{X}, \tilde{Y})$ (the reason for this assumption will be discussed below). Moreover, it is assumed that the solution depends on the scaled time variable $\tilde{\tau} = \epsilon^2 t$. In this case, the nonlinear model governing three-dimensional flows with a deformable interface can be drastically simplified by means of a long-wavelength expansion. The details of the long-wave approach applied to thermocapillary flows can be found in the review papers of Davis (1987) and Oron, Davis & Bankoff (1997).

Actually, the long-wave approach applied above is justified only in the case of a strong surface tension. A strong surface tension suppresses short-wave deformations of the surfaces; therefore the instability takes place only in the region of the long waves. Later on, we assume that $\sigma_m = \sigma_m^0 \epsilon^{-2}$, $\sigma_m^0 = O(1)$, $m = 1, 2$. Moreover, we assume that the dependence of the interfacial tensions on the temperature is relatively weak

and can be neglected in the boundary conditions for normal stresses (but not in the boundary conditions for tangential stresses where it is the source of a thermocapillary motion).

The appropriate scaling of variables for a long-scale flow governed by the system (2.1)–(2.14) is as follows:

$$(v_{mx}, v_{my}) = \epsilon \boldsymbol{V}_m + o(\epsilon), \quad v_{mz} = \epsilon^2 W_m + o(\epsilon^2), \quad p_m = P_m + o(\epsilon^2); \quad m = 1, 2. \tag{3.1a–c}$$

At the leading order, the evolution of the system is governed by the following equations and boundary conditions:

$$\left.\begin{array}{c} P_{1zz} = 0; \quad -\tilde{\boldsymbol{\nabla}}_\perp P_1 + \eta_1 \boldsymbol{V}_{1zz} = 0; \quad \tilde{\boldsymbol{\nabla}}_\perp \cdot \boldsymbol{V}_1 + W_{1z} = 0; \\ T_{1zz} = 0; \quad 0 < z < H_1(\tilde{\boldsymbol{X}}, \tilde{\tau}); \end{array}\right\} \tag{3.2}$$

$$\left.\begin{array}{c} P_{2zz} = 0; \quad -\tilde{\boldsymbol{\nabla}}_\perp P_2 + \eta_2 \boldsymbol{V}_{2zz} = 0; \quad \tilde{\boldsymbol{\nabla}}_\perp \cdot \boldsymbol{V}_2 + W_{2z} = 0; \\ T_{2zz} = 0; \quad H_1(\tilde{\boldsymbol{X}}, \tilde{\tau}) < z < H_2(\tilde{\boldsymbol{X}}, \tilde{\tau}); \end{array}\right\} \tag{3.3}$$

$$z = 0 : \boldsymbol{V}_1 = 0; \quad W_1 = 0; \quad T_1 = T_s; \tag{3.4}$$

$$z = H_1 : \boldsymbol{V}_1 = \boldsymbol{V}_2; \quad W_1 = W_2; \tag{3.5}$$

$$P_2 - P_1 - \sigma_1^0 \tilde{\boldsymbol{\nabla}}_\perp^2 H_1 = 0; \tag{3.6}$$

$$\eta_2 \boldsymbol{V}_{2z} - \eta_1 \boldsymbol{V}_{1z} - \alpha_1 (\tilde{\boldsymbol{\nabla}}_\perp T_1 + T_{1z} \tilde{\boldsymbol{\nabla}}_\perp H_1) = 0; \tag{3.7}$$

$$H_{1\tilde{\tau}} + \boldsymbol{V}_1 \cdot \tilde{\boldsymbol{\nabla}}_\perp H_1 = W_1; \tag{3.8}$$

$$T_1 = T_2; \quad \kappa_1 T_{1z} = \kappa_2 T_{2z} + Q_*; \tag{3.9}$$

$$z = H_2 : -\eta_2 \boldsymbol{V}_{2z} - \alpha_2 (\tilde{\boldsymbol{\nabla}}_\perp T_2 + T_{2z} \tilde{\boldsymbol{\nabla}}_\perp H_2) = 0; \tag{3.10}$$

$$-P_2 - \sigma_2^0 \tilde{\boldsymbol{\nabla}}_\perp^2 H_2 = 0; \tag{3.11}$$

$$H_{2\tilde{\tau}} + \boldsymbol{V}_2 \cdot \tilde{\boldsymbol{\nabla}}_\perp H_2 = W_2; \tag{3.12}$$

$$\kappa_2 T_{2z} = -q(T_2 - T_g). \tag{3.13}$$

Here, $\tilde{\boldsymbol{\nabla}}_\perp = (\partial/\partial\tilde{X}, \partial/\partial\tilde{Y})$, and the subscripts z and $\tilde{\tau}$ denote partial derivatives with respect to the corresponding variables.

Relations (3.6) and (3.11) determine expressions for the Laplace pressures,

$$P_1 = -\sigma_1 \tilde{\boldsymbol{\nabla}}_\perp^2 H_1 - \sigma_2 \tilde{\boldsymbol{\nabla}}_\perp^2 H_2, \tag{3.14}$$

$$P_2 = -\sigma_2 \tilde{\boldsymbol{\nabla}}_\perp^2 H_2. \tag{3.15}$$

Solving the problem for the temperature fields, we find

$$T_1(\tilde{\boldsymbol{X}}, \tilde{\tau}) = T_s(\tilde{\boldsymbol{X}}) - (T_s(\tilde{\boldsymbol{X}}) - T_g) D(\tilde{\boldsymbol{X}}, \tilde{\tau}) q \kappa_2 z, \tag{3.16}$$

$$T_2(\tilde{\boldsymbol{X}}, \tilde{\tau}) = T_s(\tilde{\boldsymbol{X}}) - (T_s(\tilde{\boldsymbol{X}}) - T_g) D(\tilde{\boldsymbol{X}}, \tilde{\tau}) q [(\kappa_2 - \kappa_1) H_1(\tilde{\boldsymbol{X}}, \tilde{\tau}) + \kappa_1 z], \tag{3.17}$$

where

$$D(\tilde{\boldsymbol{X}}, \tilde{\tau}) = [\kappa_1 \kappa_2 + q(\kappa_2 - \kappa_1) H_1(\tilde{\boldsymbol{X}}, \tilde{\tau}) + q \kappa_1 H_2(\tilde{\boldsymbol{X}}, \tilde{\tau})]^{-1}. \tag{3.18}$$

The horizontal components of the flow velocities $\boldsymbol{V}_m$ ($m = 1, 2$), which are generated by the thermocapillary stresses and the gradients of the Laplace pressures,

are determined by linear equations and boundary conditions. Therefore, we can present $\boldsymbol{V}_m$ as a sum of two terms $\boldsymbol{V}_m^T$ and $\boldsymbol{V}_m^\sigma$, which are related by those two factors respectively. Similarly, the vertical component of the flow velocity W_m can be presented as $W_m = W_m^T + W_m^\sigma$. Let us consider $(\boldsymbol{V}_m^T, W_m^T)$ and $(\boldsymbol{V}_m^\sigma, W_m^\sigma)$ separately.

Disregarding Laplace pressures, we obtain the following expressions for the horizontal components of the thermocapillary flows:

$$\boldsymbol{V}_1^T = -\left(\frac{\alpha_1}{\eta_1}\tilde{\boldsymbol{\nabla}}_\perp A + \frac{\alpha_2}{\eta_1}\tilde{\boldsymbol{\nabla}}_\perp B\right) z, \tag{3.19}$$

$$\boldsymbol{V}_2^T = -\frac{\alpha_1}{\eta_1} H_1 \tilde{\boldsymbol{\nabla}}_\perp A - \alpha_2 \left(\frac{z - H_1}{\eta_2} + \frac{H_1}{\eta_1}\right) \tilde{\boldsymbol{\nabla}}_\perp B, \tag{3.20}$$

where

$$A(\tilde{\boldsymbol{X}}, \tilde{\tau}) = T_s(\tilde{\boldsymbol{X}}) - (T_s(\tilde{\boldsymbol{X}}) - T_g) D(\tilde{\boldsymbol{X}}, \tilde{\tau}) q \kappa_2 H_1(\tilde{\boldsymbol{X}}, \tilde{\tau}), \tag{3.21}$$

$$B(\tilde{\boldsymbol{X}}, \tilde{\tau}) = T_s(\tilde{\boldsymbol{X}}) - (T_s(\tilde{\boldsymbol{X}}) - T_g) D(\tilde{\boldsymbol{X}}) q [(\kappa_2 - \kappa_1) H_1(\tilde{\boldsymbol{X}}) + \kappa_1 H_2(\tilde{\boldsymbol{X}})]. \tag{3.22}$$

Solving the continuity equations with respect to W_1 and W_2 with corresponding boundary conditions, we find that

$$W_1^T(\tilde{\boldsymbol{X}}, \tilde{\tau}) = -\int_0^{H_1} \tilde{\boldsymbol{\nabla}}_\perp \cdot \boldsymbol{V}_1 \, \mathrm{d}z, \tag{3.23}$$

$$W_2^T(\tilde{\boldsymbol{X}}, \tilde{\tau}) = -\int_0^{H_1} \tilde{\boldsymbol{\nabla}}_\perp \cdot \boldsymbol{V}_1 \, \mathrm{d}z - \int_{H_1}^{H_2} \tilde{\boldsymbol{\nabla}}_\perp \cdot \boldsymbol{V}_2 \, \mathrm{d}z. \tag{3.24}$$

Substituting the expressions for the flow velocities obtained above into equations (3.8) and (3.12), we arrive at a closed system of equations that governs the evolution of a heated two-layer film under the action of the thermocapillary effect:

$$H_{1\tilde{\tau}} + \tilde{\boldsymbol{\nabla}}_\perp \cdot \boldsymbol{Q}_1^T = 0, \quad H_{2\tilde{\tau}} + \tilde{\boldsymbol{\nabla}}_\perp \cdot \boldsymbol{Q}_2^T = 0. \tag{3.25a,b}$$

The expressions for the fluxes produced by the thermocapillary effect are as follows:

$$\boldsymbol{Q}_1^T = -\frac{\alpha_1 H_1^2}{2\eta_1}\tilde{\boldsymbol{\nabla}}_\perp A - \frac{\alpha_2 H_1^2}{2\eta_1}\kappa_1\kappa_2\tilde{\boldsymbol{\nabla}}_\perp C, \tag{3.26}$$

$$\boldsymbol{Q}_2^T = -\frac{\alpha_1 H_1 (2H_2 - H_1)}{2\eta_1}\tilde{\boldsymbol{\nabla}}_\perp A - \frac{\alpha_2 \kappa_1 \kappa_2}{2\eta_1 \eta_2}[H_2^2 \eta_1 + (2H_2 - H_1) H_1 (\eta_2 - \eta_1)]\tilde{\boldsymbol{\nabla}}_\perp C, \tag{3.27}$$

where

$$C = (T_s - T_g) D. \tag{3.28}$$

Equations (3.25) were formerly derived by Nepomnyashchy & Simanovskii (2007) in the case $T_s = \text{const}$.

Similarly, disregarding the thermocapillary stresses, one can calculate the velocities $(\boldsymbol{V}_m^\sigma, W_m^\sigma)$, $m = 1, 2$, and the fluxes $\boldsymbol{Q}_1^\sigma$, $\boldsymbol{Q}_2^\sigma$. Because these fluxes were computed

formerly by Pototsky *et al.* (2004), Bandyopadhyay, Gulabani & Sharma (2005) and Fisher & Golovin (2005), we present here only the final result:

$$\boldsymbol{Q}_1^\sigma = F_{11}\tilde{\boldsymbol{\nabla}}_\perp P_1 + F_{12}\tilde{\boldsymbol{\nabla}}_\perp P_2, \quad \boldsymbol{Q}_2^\sigma = F_{21}\tilde{\boldsymbol{\nabla}}_\perp P_1 + F_{22}\tilde{\boldsymbol{\nabla}}_\perp P_2, \tag{3.29}$$

where the pressures P_1 and P_2 are determined by the expressions (3.14) and (3.15), and the mobility functions are

$$\left.\begin{aligned} &F_{11} = -\frac{1}{3\eta_1}H_1^3; \quad F_{12} = -\frac{1}{2\eta_1}H_1^2(H_2 - H_1); \quad F_{21} = \frac{1}{6\eta_1}H_1^3 - \frac{1}{2\eta_1}H_1^2 H_2; \\ &F_{22} = (H_2 - H_1)\left[H_1^2\left(\frac{1}{2\eta_1} - \frac{1}{3\eta_2}\right) + H_1 H_2\left(-\frac{1}{\eta_1} + \frac{2}{3\eta_2}\right) - \frac{1}{3\eta_2}H_2^2\right]. \end{aligned}\right\} \tag{3.30}$$

Finally, we obtain the following evolution equations:

$$H_{1\tilde{\tau}} + \tilde{\boldsymbol{\nabla}}_\perp \cdot (\boldsymbol{Q}_1^T + \boldsymbol{Q}_1^\sigma) = 0, \quad H_{2\tilde{\tau}} + \tilde{\boldsymbol{\nabla}}_\perp \cdot (\boldsymbol{Q}_2^T + \boldsymbol{Q}_2^\sigma) = 0. \tag{3.31a,b}$$

Let us transform equations (3.31) to a non-dimensional form. The natural vertical length scale is the equilibrium thickness of the lower layer, H_1^0. The choice of the horizontal length scale, L^*, is arbitrary (see Nepomnyashchy & Simanovskii 2012). We choose

$$\tau^* = \frac{\eta_1 (L^*)^4}{\sigma_1^0 (H_1^0)^3} \tag{3.32}$$

as a time scale and

$$p^* = \frac{\sigma_1^0 H_1^0}{(L^*)^2} \tag{3.33}$$

as a pressure scale.

The non-dimensional parameters of the problem are the Biot number,

$$Bi = \frac{qH_1^0}{\kappa_2}, \tag{3.34}$$

$\eta = \eta_1/\eta_2$, $\kappa = \kappa_1/\kappa_2$, $\sigma = \sigma_2^0/\sigma_1^0$ and $\alpha = \alpha_2/\alpha_1$. We define non-dimensional variables

$$\boldsymbol{X} = \tilde{\boldsymbol{X}}/L^*, \quad \tau = \tilde{\tau}/\tau^*, \quad h_j = H_j/H_1^0, \quad \pi_j = P_j/p^*, \quad j = 1, 2. \tag{3.35a–d}$$

We introduce also the local modified Marangoni number,

$$M(\boldsymbol{X}) = \frac{\alpha_1 (T_s(\boldsymbol{X}) - T_g)}{\sigma_1^0}\left(\frac{L^*}{H_1^0}\right)^2 \tag{3.36}$$

and

$$d(\boldsymbol{X}, \tau) = [\kappa + Bi(1-\kappa)h_1(\boldsymbol{X}, \tau) + Bi\kappa h_2(\boldsymbol{X}, \tau)]^{-1}. \tag{3.37}$$

Equations (3.31) written in the non-dimensional form look as follows:

$$h_{1\tau} + \boldsymbol{\nabla}_\perp \cdot \boldsymbol{q}_1 = 0, \quad h_{2\tau} + \boldsymbol{\nabla}_\perp \cdot \boldsymbol{q}_2 = 0, \tag{3.38a,b}$$

$$\boldsymbol{q}_1 = f_{11}\boldsymbol{\nabla}_\perp p_1 + f_{12}\boldsymbol{\nabla}_\perp p_2 + \boldsymbol{q}_1^T, \quad \boldsymbol{q}_2 = f_{21}\boldsymbol{\nabla}_\perp p_1 + f_{22}\boldsymbol{\nabla}_\perp p_2 + \boldsymbol{q}_2^T, \tag{3.39a,b}$$

where

$$f_{11} = -\tfrac{1}{3}h_1^3, \quad f_{12} = -\tfrac{1}{2}h_1^2(h_2 - h_1), \tag{3.40a,b}$$

$$f_{21} = \frac{1}{6}h_1^3 - \frac{1}{2}h_1^2 h_2, \quad f_{22} = (h_2 - h_1)\left[h_1^2\left(\frac{1}{2} - \frac{\eta}{3}\right) + h_1 h_2\left(-1 + \frac{2\eta}{3}\right) - \frac{\eta}{3}h_2^2\right]. \tag{3.41a,b}$$

The capillary pressures are

$$\pi_1 = -\nabla_\perp^2 h_1 - \sigma\nabla_\perp^2 h_2, \tag{3.42}$$

$$\pi_2 = -\sigma\nabla_\perp^2 h_2. \tag{3.43}$$

The non-dimensional expressions for the fluxes generated by the thermocapillary effect are

$$\boldsymbol{q}_1^T = -\frac{h_1^2}{2}\boldsymbol{\nabla}_\perp\{M[1 + d(\alpha\kappa - Bih_1)]\}, \tag{3.44}$$

$$\boldsymbol{q}_2^T = -\frac{\eta\alpha\kappa}{2}h_2^2\boldsymbol{\nabla}_\perp(Md) + \frac{(2h_2 - h_1)h_1}{2}\boldsymbol{\nabla}_\perp\{M[-1 + Bih_1 d - \alpha\kappa(1-\eta)d]\}. \tag{3.45}$$

4. Nonlinear simulations

4.1. *Methodology*

We have performed nonlinear simulations of equations (3.38) with a spatially periodic modulation of the Marangoni number,

$$M(X + L, Y) = M(X, Y + L) = M(X, Y). \tag{4.1}$$

Let us emphasize that L is a non-dimensional parameter; the dimensional modulation period is $\tilde{L} = LL^*$. Equations (3.38)–(3.45) have been discretized by central differences for spatial derivatives and solved using an explicit scheme. Initial conditions for h_j, $j = 1, 2$, have been chosen in such a way that the mean value of $h_1(X, Y, 0)$ is equal to 1 and the mean value of $h_2(X, Y, 0)$ is equal to h, where $h > 1$. It should be noted that the solutions of the problem depend on the additional geometric parameter, $h = H_2^0/H_1^0$. Small random deviations of $h_j(X, Y, 0)$ from their mean values were imposed using a code creating pseudo-random numbers. The computations were performed in the region $L \times L = 240 \times 240$ with periodic boundary conditions using a grid of 80×80. In this paper, we consider the system of fluorinert FC70 (liquid 1) and silicone oil 10 (liquid 2) formerly used in microgravity experiments (see, e.g., Géoris *et al.* 1999). It is characterized by the following set of parameters: $\eta = 3.04$, $\kappa = 0.522$, $\alpha = 2$, $\rho = 0.482$, $\sigma = 2.6$. The computations are carried out for $h = 2.5$ and $Bi = 10$.

The primary analysis of the obtained nonlinear regimes has been performed using snapshots of the fields of $h_j(X, Y, \tau)$, $j = 1, 2$. This analysis has been supplemented by the investigation of the Fourier components

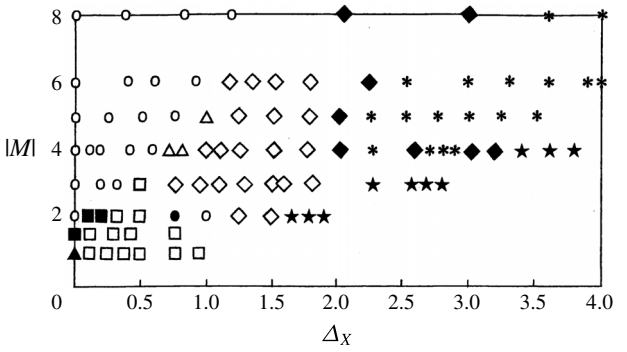

FIGURE 2. General diagram of regimes on the plane (Δ_X, M): black triangle, mechanical equilibrium; white circle, time-periodic three-dimensional standing wave; white triangle, quasiperiodic three-dimensional standing wave; black square, two-dimensional standing wave; white square, two-dimensional stationary pattern; black circle, three-dimensional travelling wave; white diamond, time-periodic standing wave with spatial period $L/2$; big star, travelling wave with spatial period $L/2$; black diamond, quasiperiodic wave with spatial period $L/2$; asterisk, standing wave with spatial period $L/3$.

$$c_{mn}(\tau) = \frac{2}{L^2}\int_0^L\int_0^L h_1(X, Y, \tau)\cos\left[\frac{2\pi}{L}(mX+nY)\right]\mathrm{d}X\,\mathrm{d}Y, \tag{4.2}$$

$$s_{mn}(\tau) = \frac{2}{L^2}\int_0^L\int_0^L h_1(X, Y, \tau)\sin\left[\frac{2\pi}{L}(mX+nY)\right]\mathrm{d}X\,\mathrm{d}Y, \tag{4.3}$$

where m, n are integer numbers.

We have used also variables

$$r_{mn}(\tau) = \sqrt{c_{mn}^2(\tau) + s_{mn}^2(\tau)}, \tag{4.4}$$

characterizing the amplitudes of the corresponding complex Fourier harmonics, and quantities

$$h_{max,j}(\tau) = \max_{X,Y} h_j(X, Y, \tau), \quad j = 1, 2, \tag{4.5}$$

which describe the deformations of the surfaces.

4.2. *One-dimensional spatial modulation with period L*

In this subsection, we discuss the nonlinear regimes observed in the case of a one-dimensional modulation of the local Marangoni number,

$$M(\boldsymbol{X}) = M\left(1 + \delta_X \sin\frac{X}{L}\right) = M - \Delta_X \sin\frac{X}{L}, \tag{4.6}$$

where $M < 0$, $\delta_X > 0$ and $\Delta_X = |M|\delta_X$. The diagram of regimes is shown in figure 2.

4.2.1. *Nonlinear regime in the absence of modulation*

The stability of the mechanical equilibrium, and the nonlinear flow regimes in the absence of the substrate temperature modulation ($\Delta_X = 0$) have been studied

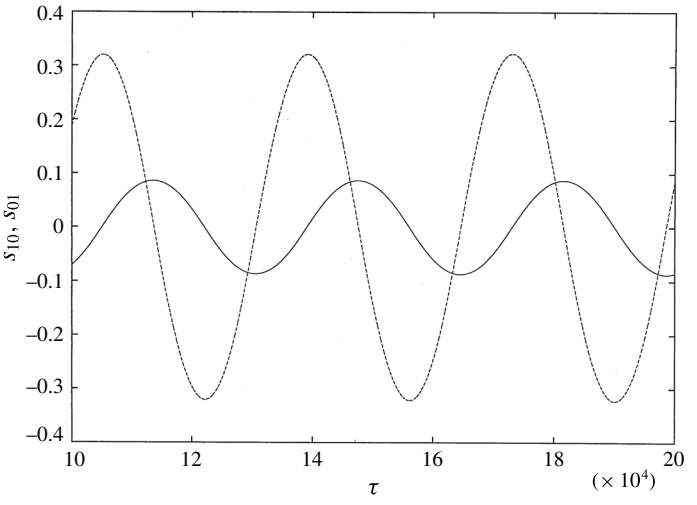

FIGURE 3. Oscillations of $s_{10}(\tau)$ (solid line) and s_{01} (dashed line) for $M = -2$, $\Delta_X = 0$.

by Nepomnyashchy & Simanovskii (2012). For $Bi = 10$, the mechanical equilibrium state is unstable with respect to oscillatory disturbances by heating from above. For the region $L \times L = 240 \times 240$ with periodic boundary conditions, the linear stability theory predicts the instability threshold $M_* \approx 1.02$. Below the threshold, the system tends to the mechanical equilibrium state. Just above the threshold, the nonlinear development of the instability creates a two-dimensional time-periodic standing wave with the wavevectors directed either along the X axis or along the Y axis (see the black square in figure 2). With the growth of $|M|$, we observe a transition to the wavy pattern known as alternating rolls. This motion is a superposition of two periodic standing waves with the wavevectors directed along the axes X, Y. The oscillations of waves with orthogonal wavevectors have a mutual phase shift corresponding to a quarter of the period, $T/4$ (see figure 3). The mean values of the Fourier components $s_{10}(\tau)$, $c_{10}(\tau)$, $s_{01}(\tau)$, $c_{01}(\tau)$ are equal to zero; the amplitudes of both standing waves are equal,

$$\max_{\tau} r_{10}(\tau) = \max_{\tau} r_{01}(\tau). \tag{4.7}$$

The quantities $h_{max,j}(\tau)$, $j = 1, 2$, oscillate with the period $T/4$ (see figure 4).

4.2.2. *Two-dimensional stationary flow*

As mentioned above, in the absence of modulation no flow is observed in the subcritical region $|M| < M_*$. The inhomogeneity of the substrate temperature generates a two-dimensional stationary flow (3.19), (3.20), and that flow creates a two-dimensional stationary deformation of the surfaces $h_j = h_j(x)$, $j = 1, 2$. For this solution, $c_{10} = 0$ and $s_{10} = \text{const}$; all c_{mn}, s_{mn} with $n \neq 0$ are equal to zero. In figure 2, this regime occupies the region indicated by white squares. For moderate values of Δ_X, the stationary flow generated by temperature modulation is more stable than the mechanical equilibrium in the absence of modulation: it is observed up to $|M| \approx 3$. Isolines of $h_2(X, Y) - h$ for this flow are shown in figure 5.

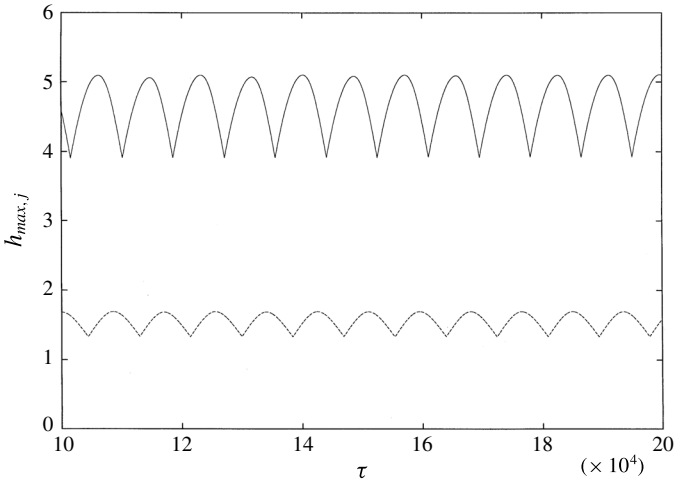

FIGURE 4. Oscillations of $h_{max,1}(\tau)$ (dashed line) and $h_{max,2}(\tau)$ (solid line) for $M = -2$, $\Delta_X = 0$.

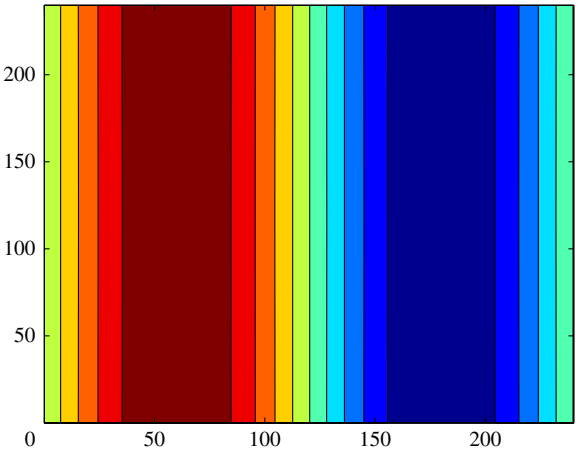

FIGURE 5. (Colour online) Isolines of $h_2(X, Y) - h$; $M = -2$, $\Delta_X = 0.5$.

4.2.3. *Two-dimensional standing waves*

The instability of a two-dimensional stationary flow can lead to the development of two-dimensional standing waves. In this regime, $s_{10}(\tau)$ oscillates with a non-zero mean value, while c_{mn}, s_{mn} with $n \neq 0$ are equal to zero (see figure 6).

The quantities $h_{max,j}$, $j = 1, 2$, oscillate with the period T, and they have two maxima during the period (see figure 7).

It should be noted that the selection of the phase of the standing wave ($c_{10}(\tau) \to 0$) is an extremely slow process. This process is shown in figure 8 for $\Delta_X = 0.2$. For smaller values of Δ_X, it is even slower.

The region of two-dimensional standing waves is indicated in figure 2 by black squares.

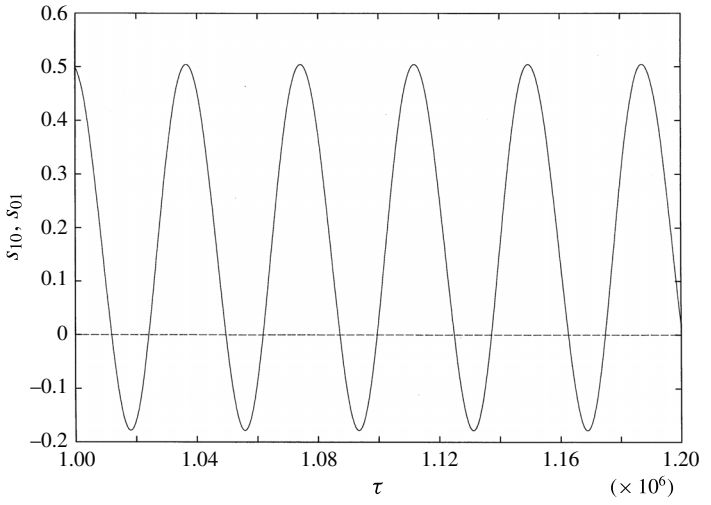

FIGURE 6. The temporal dependence of $s_{10}(\tau)$ (solid line) and $s_{01}(\tau)$ (dashed line) for $M = -2,\ \Delta_X = 0.2$.

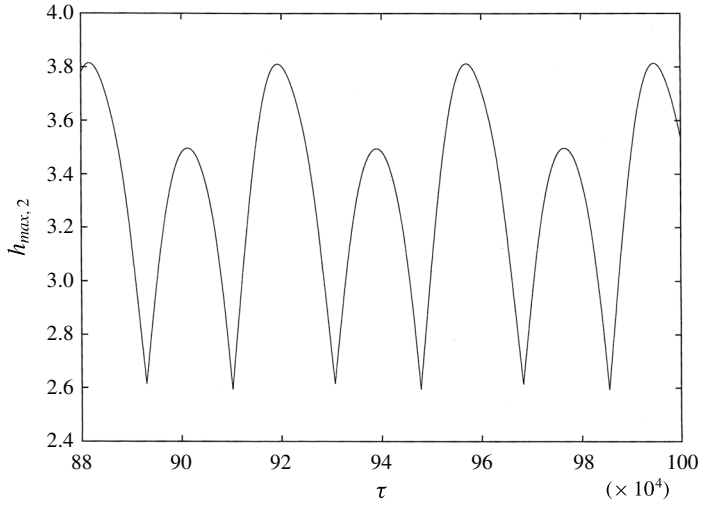

FIGURE 7. Oscillations of $h_{max,2}(\tau)$ for $M = -2,\ \Delta_X = 0.2$.

4.2.4. *Three-dimensional standing waves*

The most typical nonlinear regime at moderate values of Δ_X is the regime of three-dimensional standing waves, which are developed due to the influence of modulation on the alternating rolls.

The non-uniformity of heating determined by (4.1) breaks (i) the translational symmetry along the X axis and (ii) the symmetry between standing waves with wavevectors directed along the X and Y axes. While for $\Delta_X = 0$ the phase of the standing wave $(s_{10}(\tau), c_{10}(\tau))$, $\phi = \tan^{-1}(c_{10}/s_{10})$, is arbitrary, in the case $\Delta_X \neq 0$ a definite value of ϕ is selected. Typically, $c_{10}(\tau) \to 0$, i.e. $\phi = 0$ is selected, but the transition to the equilibrium value of the phase is a very slow process. The imposed

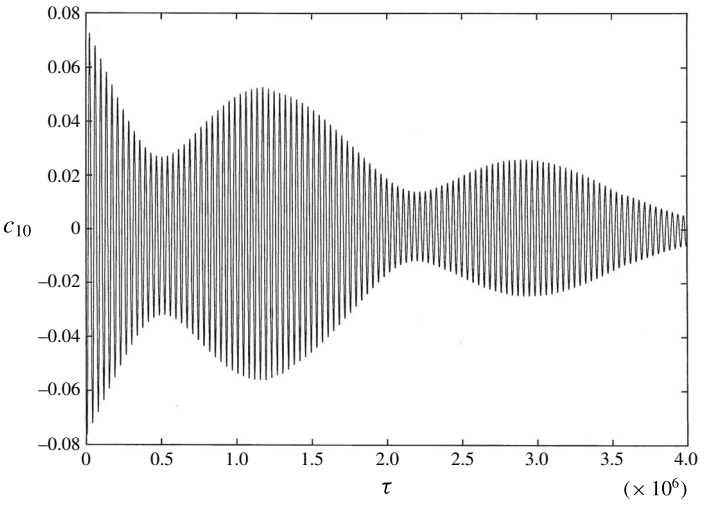

FIGURE 8. Decay of $c_{10}(\tau)$ for $M = -2$, $\Delta_X = 0.2$.

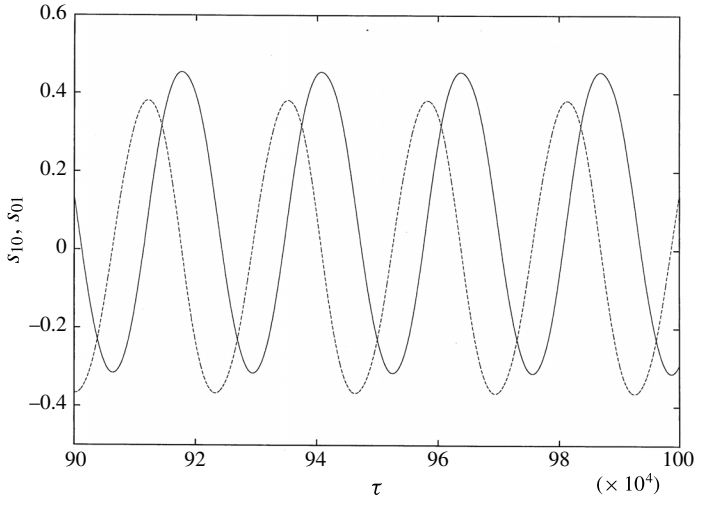

FIGURE 9. Oscillations of $s_{10}(\tau)$ (solid line) and $s_{01}(\tau)$ (dashed line) for $M = -3$, $\Delta_X = 0.15$.

temperature non-uniformity generates a thermocapillary flow, which creates a certain mean deformation of surfaces. Therefore, the mean value of $s_{10}(\tau)$ is non-zero (see figure 9), and it increases with the growth of Δ_X. The phase of the standing wave $(s_{01}(\tau), c_{01}(\tau))$ is arbitrary, the mean values of $s_{01}(\tau)$ and $c_{01}(\tau)$ are equal to zero (figure 9) and the amplitude of this standing wave decreases with the growth of Δ_X.

The phase trajectory in the plane (r_{10}, r_{01}) is shown in figure 10. One can see that each of the functions $r_{10}(\tau)$, $r_{01}(\tau)$ has two different local maxima during the period. The quantities $h_{max,j}$, $j = 1, 2$, oscillate now with the period T, but they have four non-equal maxima during the period (see figure 11).

The regime of time-periodic three-dimensional standing waves described above is observed in a large region in the plane (Δ_X, M) (see figure 2, white circles).

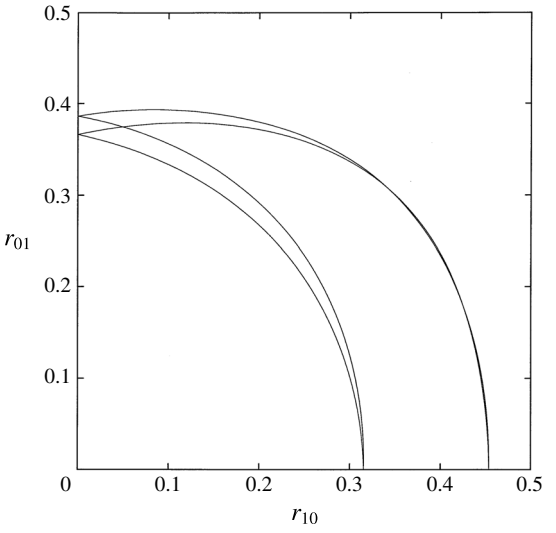

FIGURE 10. Phase trajectory in the plane (r_{10}, r_{01}) for $M = -3$, $\Delta_X = 0.15$.

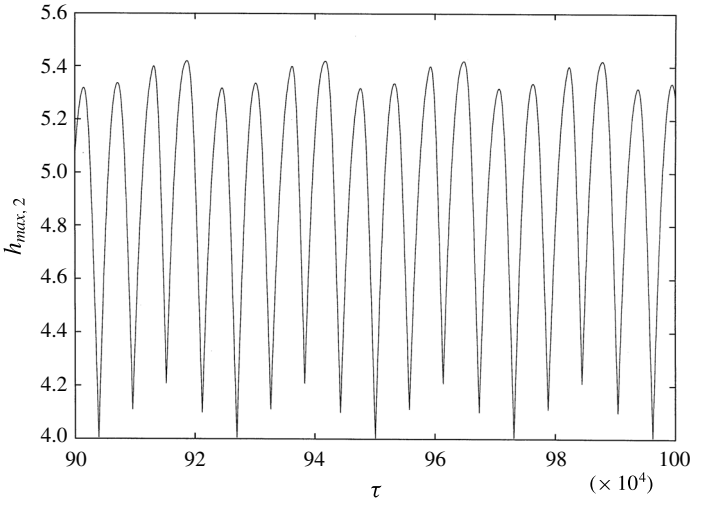

FIGURE 11. Oscillations of $h_{max,2}(\tau)$ for $M = -3$, $\Delta_X = 0.15$.

With the growth of Δ_X, the frequencies of standing waves with the wavevectors directed along the X and Y axes become different from each other (see figure 12). The region of these quasiperiodic oscillations is shown in figure 2 by white triangles.

4.2.5. *Three-dimensional travelling waves*

When Δ_X increases, the stationary flow described in § 4.2.2 becomes unstable with respect to three-dimensional oscillatory disturbances with the period L in the Y-direction. The instability creates travelling waves propagating in the Y-direction:

$$h_j(X, Y, \tau) = h_j^{\pm}(X, Y \pm c\tau), \tag{4.8}$$

where c is the phase velocity of the wave (see figure 13).

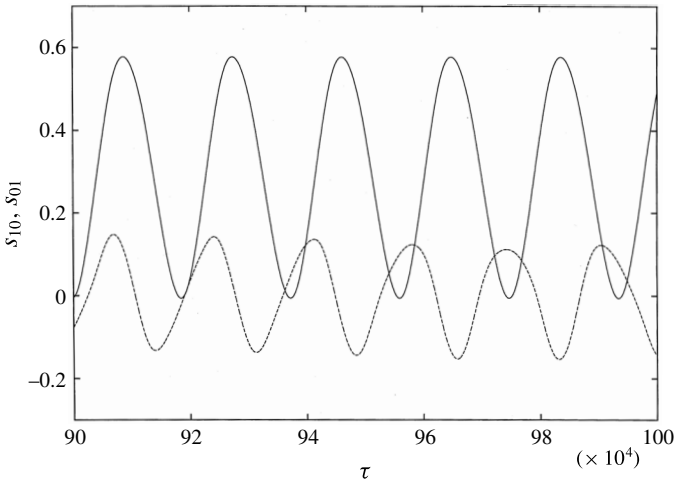

FIGURE 12. Oscillations of $s_{10}(\tau)$ (solid line) and s_{01} (dashed line) for $M=-4$, $\Delta_X=0.7$.

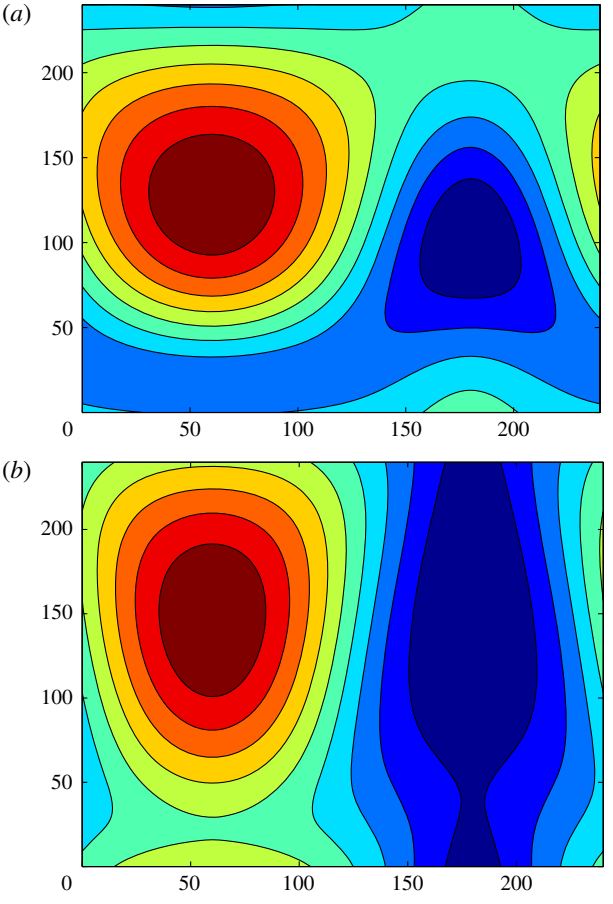

FIGURE 13. (Colour online) Snapshots of the isolines of (*a*) $h_2(X, Y, \tau) - h$ and (*b*) $h_1(X, Y, \tau) - 1$; $M=-2$, $\Delta_X=0.7$.

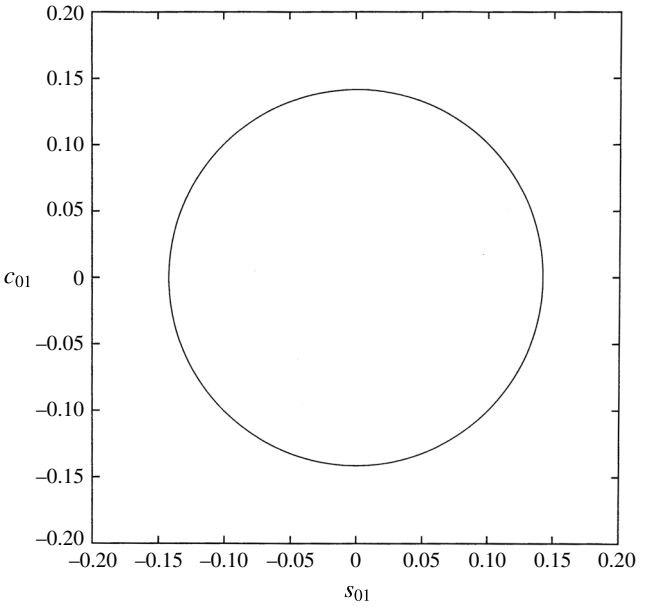

FIGURE 14. The phase trajectory in the plane s_{01}, c_{01}; $M = -2$, $\Delta_X = 0.75$.

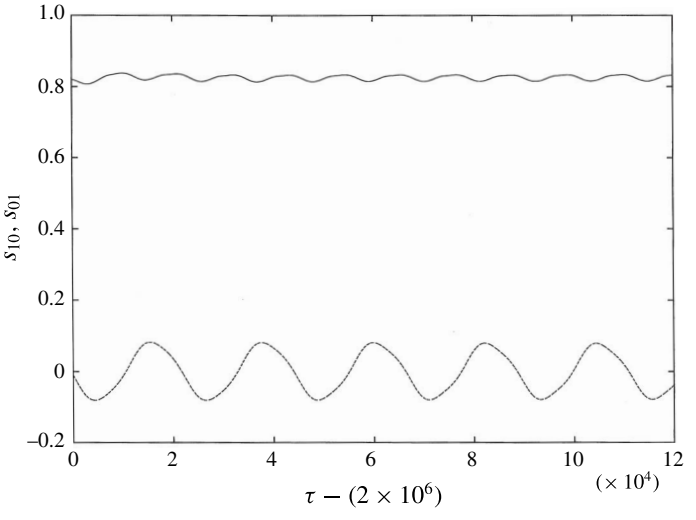

FIGURE 15. Oscillations of $s_{10}(\tau)$ (solid line) and $s_{01}(\tau)$ (dashed line) for $M = -2$, $\Delta_X = 1$. The indicated values of time correspond to $\tau - 2 \times 10^6$.

For the travelling wave solutions, $c_{10} = 0$, $s_{10} = const$, $r_{01}^2 = c_{01}^2(\tau) + s_{01}^2(\tau) = const$ (see figure 14).

4.2.6. *Re-entrant three-dimensional standing waves*

At higher values of Δ_X, we have observed the transition to the regime of standing waves with almost proportional $c_{01}(\tau)$ and $s_{01}(\tau)$. Through the nonlinear terms in the equations, the T-periodic oscillations of $c_{01}(\tau)$ and $s_{01}(\tau)$ induce oscillations of s_{10} with the period $T/2$ (see figure 15).

The snapshots of the isolines of $h_2(X, Y, \tau) - h$ are shown in figure 16.

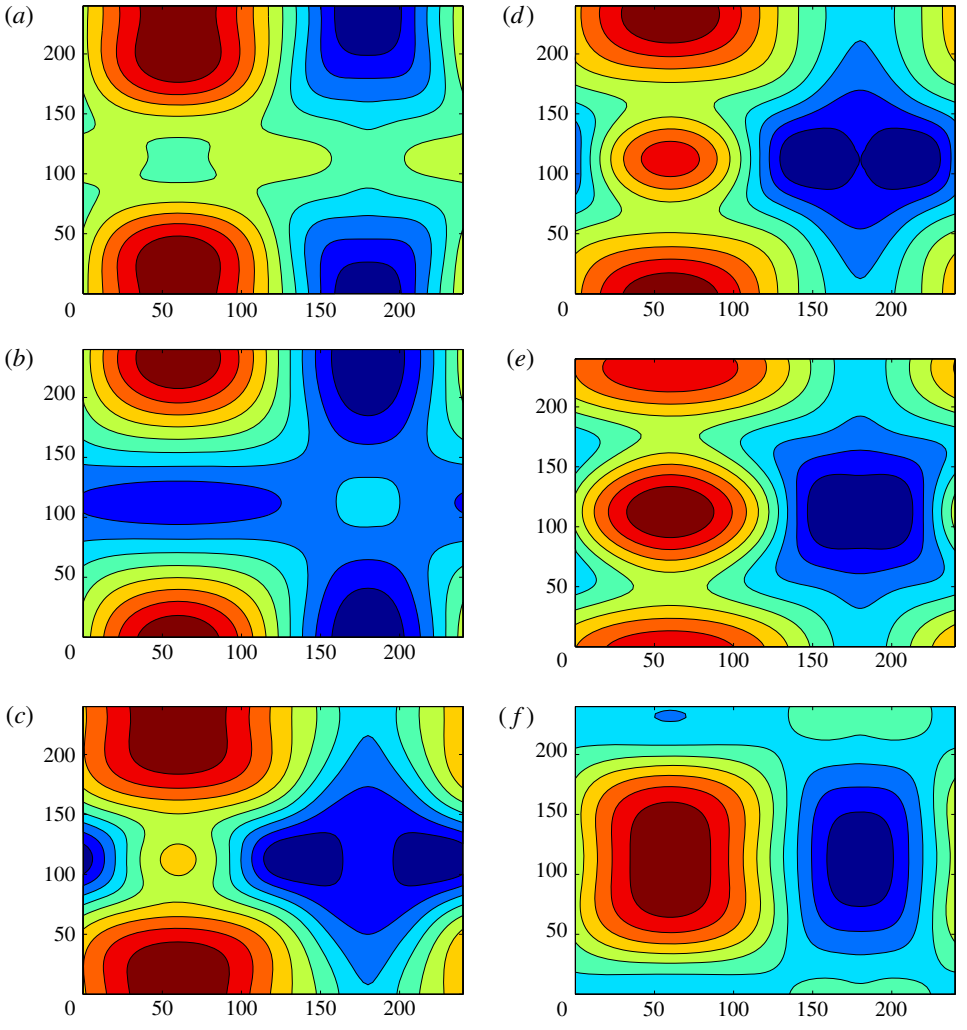

FIGURE 16. (Colour online) Snapshots of the isolines of $h_2(X, Y, \tau) - h$: (*a*) $\tau = 2\,300\,640$, (*b*) $\tau = 2\,302\,400$, (*c*) $\tau = 2\,308\,000$, (*d*) $\tau = 2\,308\,800$, (*e*) $\tau = 2\,310\,200$, (*f*) $\tau = 2\,312\,400$; $M = -2$, $\Delta_X = 1$.

4.2.7. *Short-scale three-dimensional structures*

For larger values of Δ_X, the stationary two-dimensional flow becomes unstable with respect to three-dimensional oscillatory disturbances with the spatial period $L/2$ in the Y-direction. Its nonlinear development creates a time-periodic regime of standing waves with c_{02} proportional to s_{02} (see figure 17). Due to the cubic nonlinearity in the equation, oscillations of c_{02} and s_{02} generate oscillations of s_{10} with a doubled frequency, i.e. with a temporal period that is two times smaller than that of (c_{02}, s_{02}) (see figure 18). The snapshots of the isolines for this regime are shown in figures 19 and 20. It should be noted that the fields of $h_j(X, Y)$ are symmetric with respect to some horizontal axes. The shapes of the upper surface and the interface between the liquids are presented in figure 21.

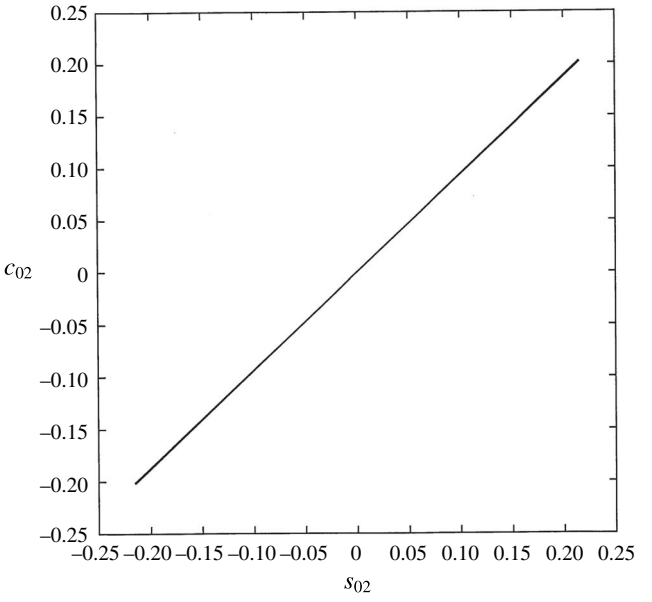

FIGURE 17. The phase trajectory in the plane s_{02}, c_{02}; $M = -4$, $\Delta_X = 1$.

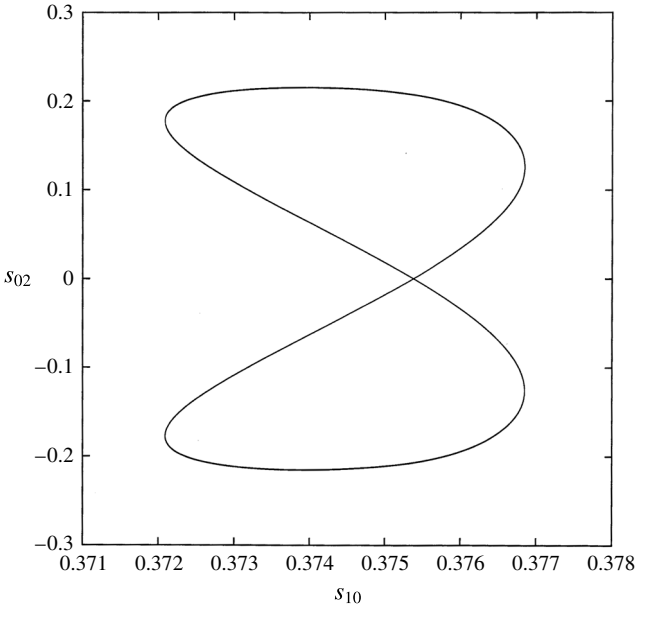

FIGURE 18. The phase trajectory in the plane s_{10}, s_{02}; $M = -4$, $\Delta_X = 1$.

At larger values of $\delta_X = \Delta_X/M$, we observe travelling waves similar to those described in § 4.2.5 (see formula (4.8)), but with the spatial period $L/2$ in the Y-direction. The symmetry of $h_j(X, Y)$ with respect to horizontal axes is broken. The snapshots of the waves moving in the direction opposite to the direction of the Y axis are shown in figure 22.

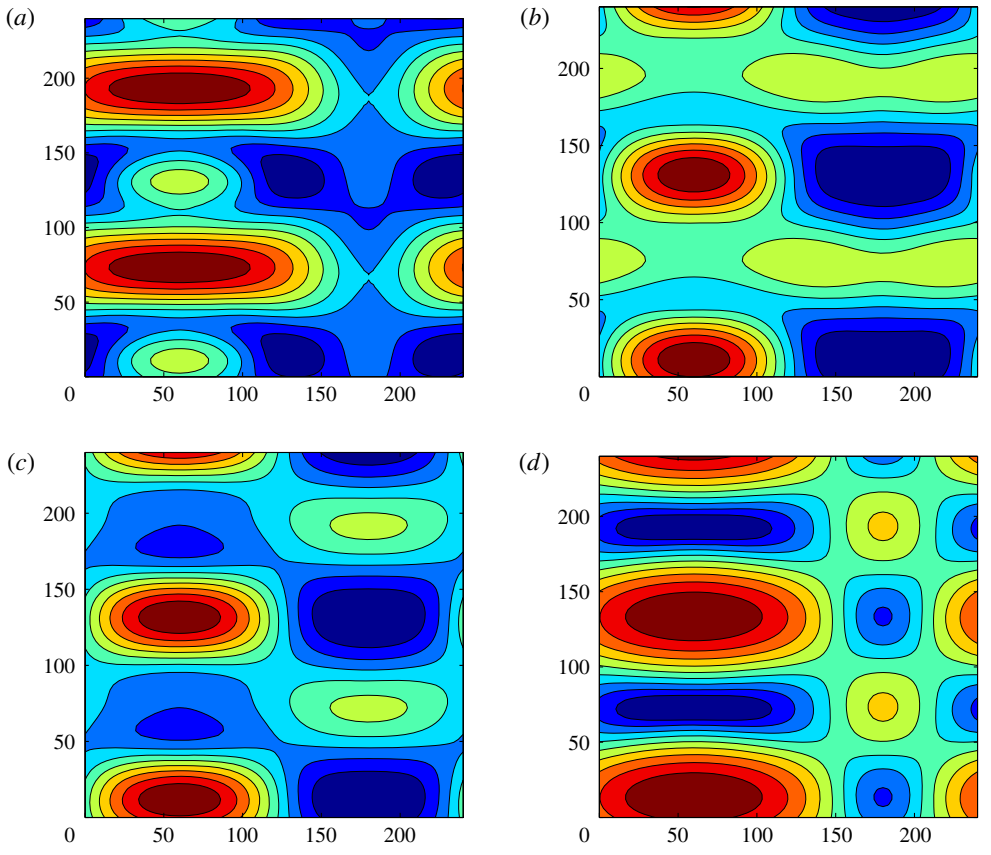

FIGURE 19. (Colour online) Snapshots of the isolines of $h_2(X, Y, \tau) - h$: (*a*) $\tau = 2\,199\,805$, (*b*) $\tau = 2\,200\,100$, (*c*) $\tau = 2\,200\,250$, (*d*) $\tau = 2\,201\,050$; $M = -4$, $\Delta_X = 1$.

In a certain region of parameters, we observe a wave that can be considered as an intermediate structure between a standing wave and a travelling wave. Similarly to the case of a standing wave, $r_{02} = \sqrt{c_{02}^2 + s_{02}^2}$ and $r_{10} = |s_{10}|$ (note that $c_{10} = 0$) oscillate periodically with the same temporal period T (see figure 23), but now r_{02} is never equal to 0. The fields $h_j(X, Y, \tau)$, which have a spatial period $L/2$ in the Y-direction (see figures 24 and 25), satisfy the relation

$$h_j(X, Y, \tau + T) = h_j(X, Y + l, \tau), \tag{4.9}$$

where l and L are generally non-commensurate. Therefore, $h_{max,j}(\tau)$ are periodic functions (see figure 26), while $c_{02}(\tau)$ and $s_{02}(\tau)$ are quasiperiodic functions of τ (see figure 26).

For $M = -6$, $\Delta_X = 3$ we have observed a structure with a spatial period $L/3$ in the Y-direction (see figures 28–30). The dynamics of the regime is fully similar to that found for $M = -4$, $\Delta_X = 1$: c_{03} and s_{03} are proportional, and s_{10} oscillates with a doubled frequency with respect to that of (c_{03}, s_{03}).

The existence regions of the regimes described above are shown in figure 2.

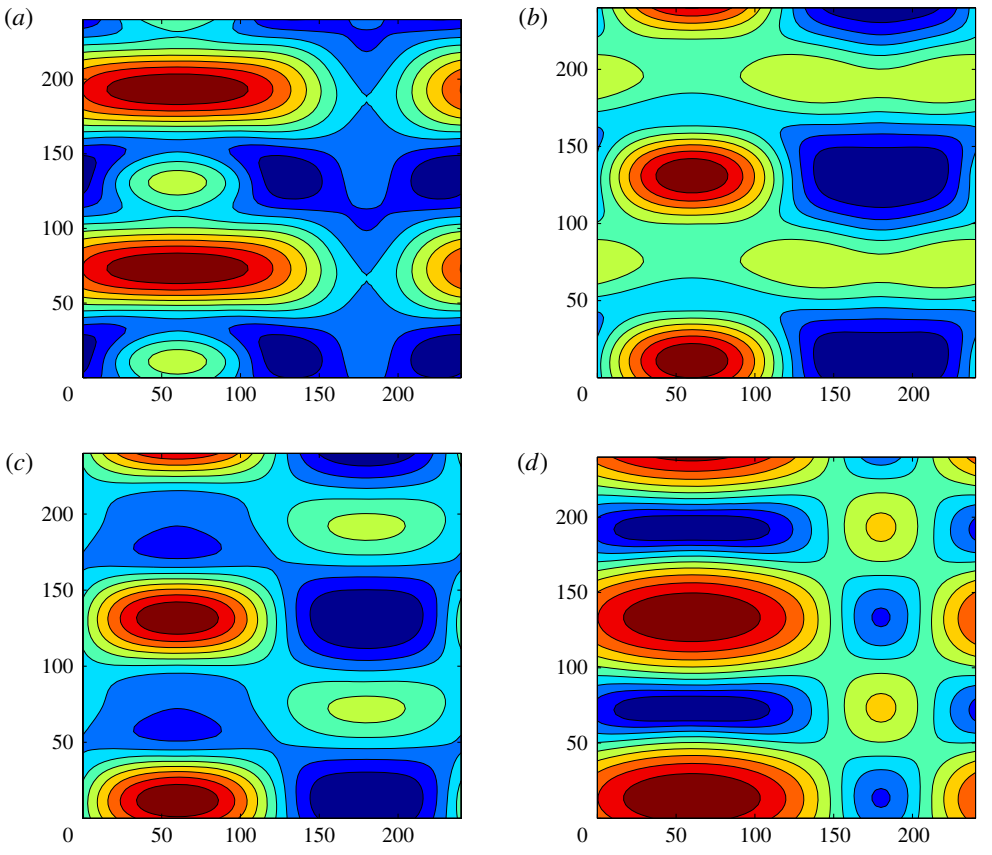

FIGURE 20. (Colour online) Snapshots of the isolines of $h_1(X, Y, \tau) - 1$: (*a*) $\tau = 2\,199\,805$, (*b*) $\tau = 2\,200\,100$, (*c*) $\tau = 2\,200\,250$, (*d*) $\tau = 2\,201\,050$; $M = -4$, $\Delta_X = 1$.

4.3. *Two-dimensional spatial modulation with period L*

Let us discuss now the modification of the basic dynamical regimes described above in the presence of a two-dimensional spatial temperature modulation,

$$M(\boldsymbol{X}) = M\left(1 + \delta_X \sin\frac{X}{L} + \delta_Y \sin\frac{Y}{L}\right) = M - \Delta_X \sin\frac{X}{L} - \Delta_Y \sin\frac{Y}{L}, \qquad (4.10)$$

where $M < 0$, $\delta_X > 0$, $\delta_Y > 0$; $\Delta_X = |M|\delta_X$, $\Delta_Y = |M|\delta_Y$. Because of the symmetry of the region, it is sufficient to consider the case $\Delta_Y \geqslant \Delta_X$.

4.3.1. *Stationary flow*

First, consider the stationary flow generated by the non-uniform distribution of the Marangoni number (4.1). The two-dimensional stationary deformation of surfaces $h_j = h_j(X, Y)$, $j = 1, 2$, reflects the spatial symmetry of the perturbation (4.1). In the case $\Delta_X = \Delta_Y$, a square pattern is imposed (see figure 30). It should be recalled that in the case $\Delta_X \neq 0$, $\Delta_Y = 0$, the pattern is one-dimensional (see figure 5).

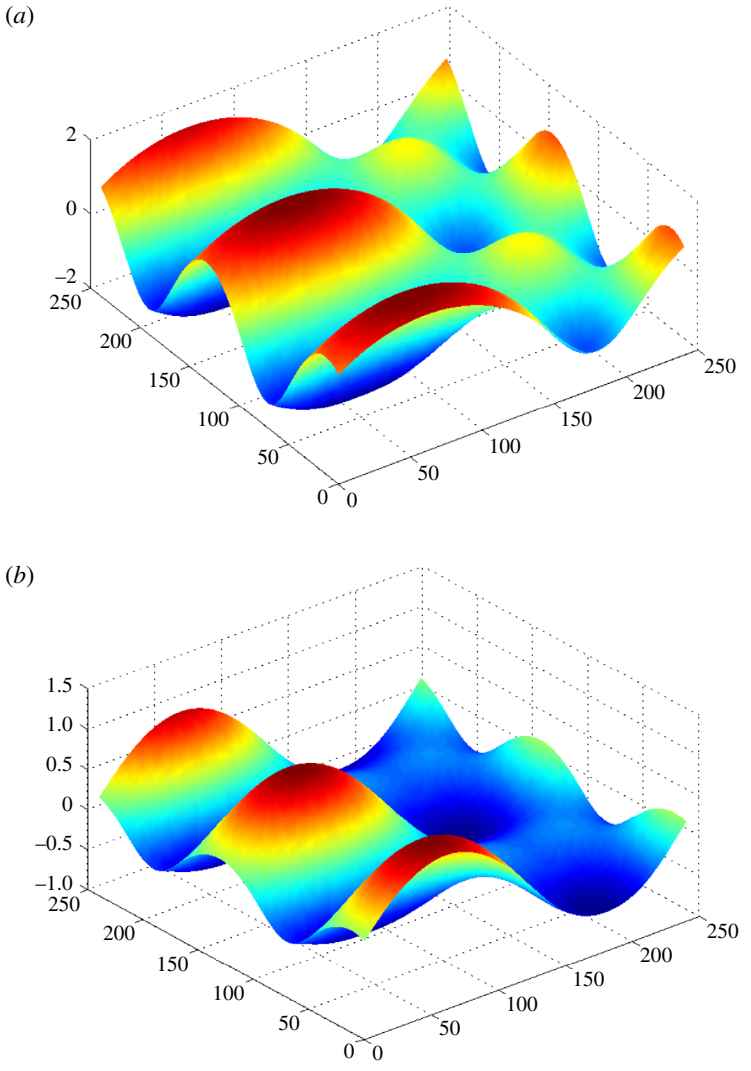

FIGURE 21. (Colour online) Shapes of (*a*) the upper surface $z = h_2(X, Y, \tau)$ and (*b*) the interface $z = h_1(X, Y, \tau)$; $M = -4$, $\Delta_X = 1$.

4.3.2. *Standing waves*

With the growth of Δ_Y, the stationary regime becomes unstable with respect to a periodic standing wave characterized by vanishing $c_{10}(\tau) = c_{01}(\tau) = 0$. The basic harmonics $s_{10}(\tau)$ and $s_{01}(\tau)$ oscillate with the same period (see figure 31). The snapshots of the oscillations are shown in figure 32.

4.4. *One-dimensional spatial modulation with period $L/2$*

An interesting resonant phenomenon has been observed in the case where the wavelength of the temperature modulation is half of the length of the region, i.e.

$$M(\boldsymbol{X}) = M - \Delta_X \sin \frac{2X}{L}. \tag{4.11}$$

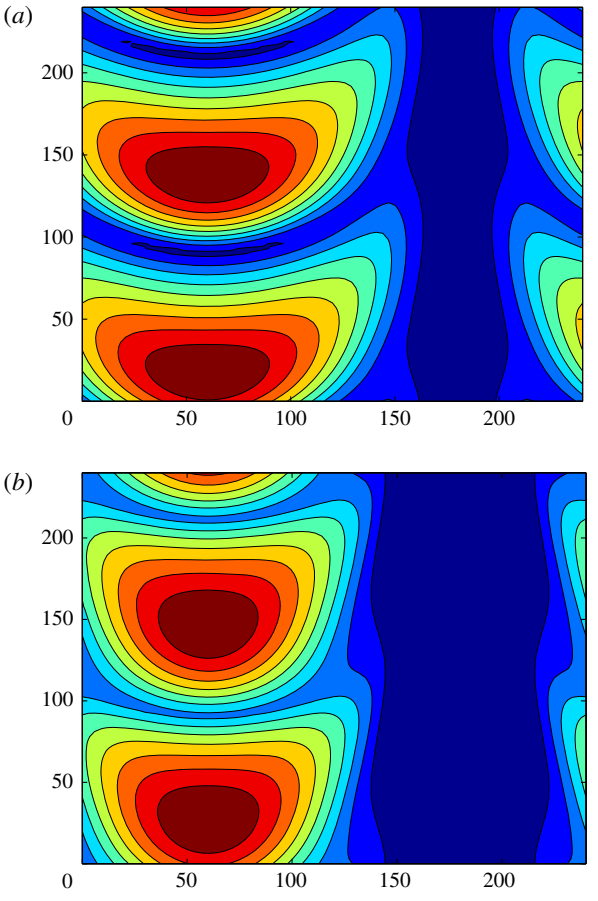

FIGURE 22. (Colour online) Snapshots of the isolines of (*a*) $h_2(X, Y, \tau) - h$ and (*b*) $h_1(X, Y, \tau) - 1$; $M = -2$, $\Delta_X = 0.7$.

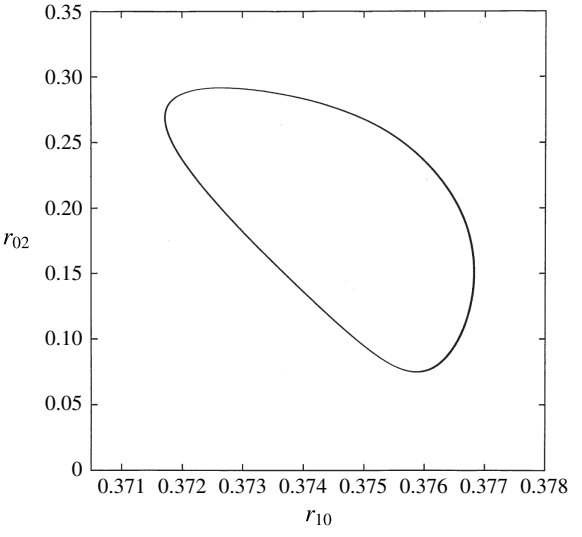

FIGURE 23. The phase trajectory in the plane r_{10}, r_{02}; $M = -8$, $\Delta_X = 2$.

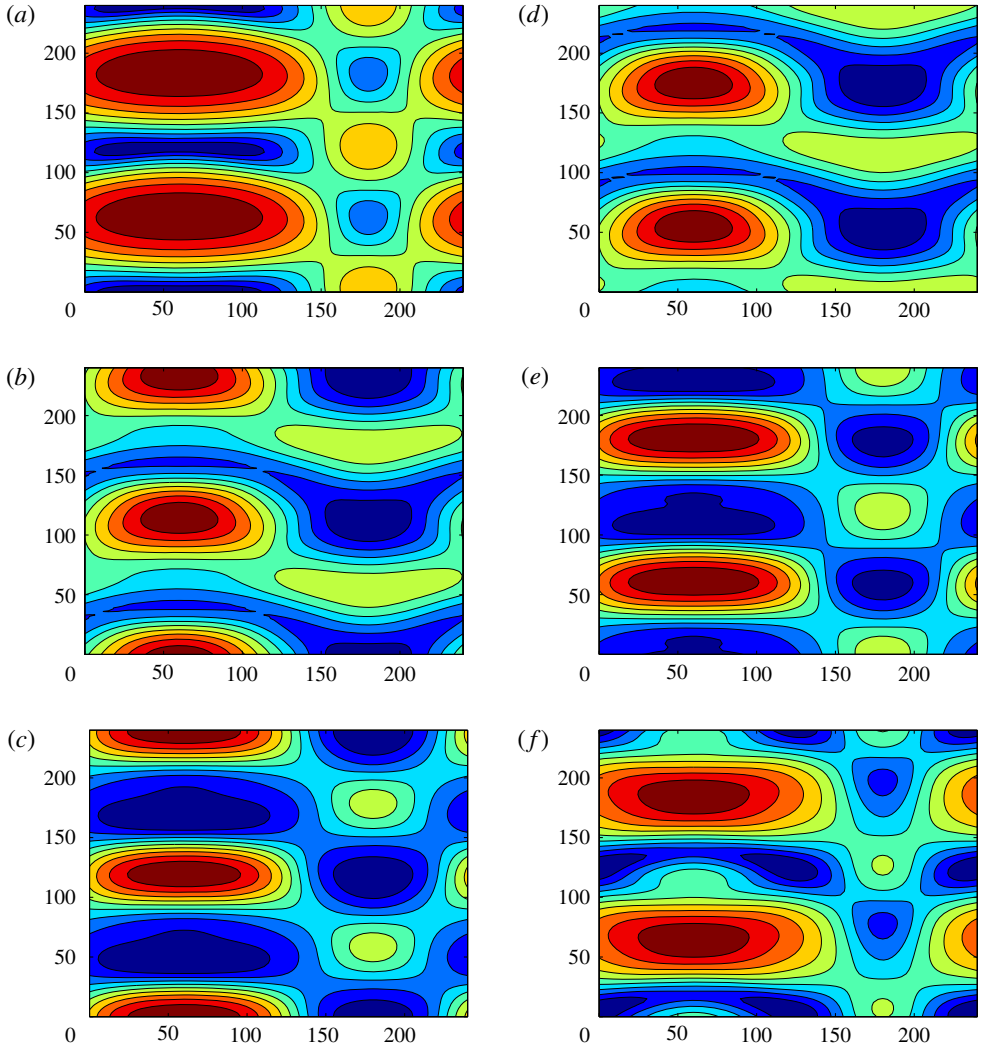

FIGURE 24. (Colour online) Snapshots of the isolines of $h_2(X, Y, \tau) - h$; $M = -8$, $\Delta_X = 2$. (*a*) $\tau = 2\,050\,000$; (*b*) $\tau = 2\,050\,420$; (*c*) $\tau = 2\,050\,620$; (*d*) $\tau = 2\,051\,340$; (*e*) $\tau = 2\,051\,600$; (*f*) $\tau = 2\,051\,980$.

The imposed temperature modulation creates a thermocapillary flow that generates the deformations of surfaces described by the Fourier component s_{20}. For instance, at $M = -1$, $\Delta_X = 0.75$ we observe stationary deformations with period $L/2$. However, because of the nonlinearity of the governing equations, that stationary flow can become unstable with respect to the excitation of the modes characterized by the Fourier components $c_{10}(\tau)$ and $s_{10}(\tau)$ ('spatial parametric resonance'), which oscillate on the background of the s_{20} mode. Due to the nonlinear interaction, the oscillations of $c_{10}(\tau)$ and $s_{10}(\tau)$ are completely synchronized (see figure 34).

The flow is two-dimensional, i.e. all of the Fourier components c_{mn} and s_{mn} vanish for $n \neq 0$. The snapshots of the two-dimensional standing wave are shown in figure 35. Typically, the wave has one maximum and one minimum, due to the Fourier components $s_{10}(\tau) = c_{10}(\tau)$ (see figure 35*a*,*b*,*d*). At the time instants when

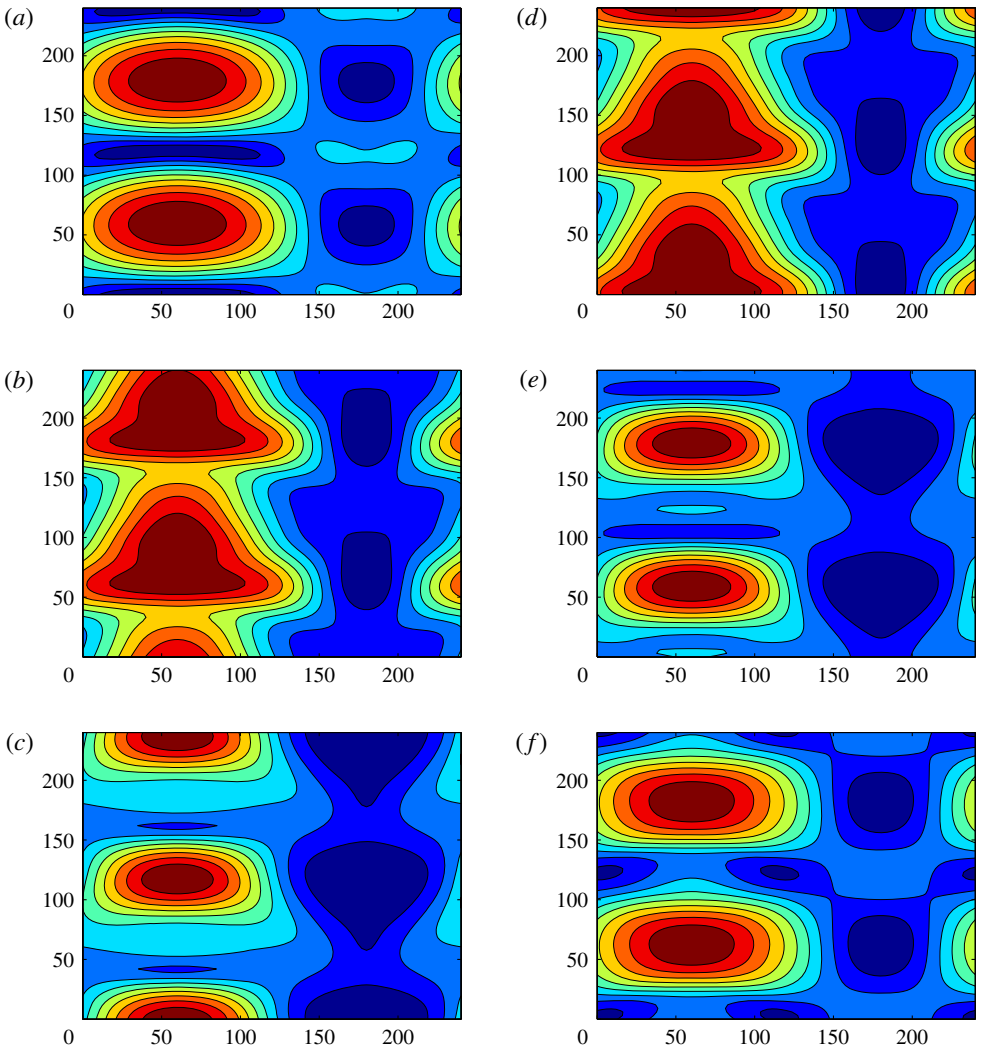

FIGURE 25. (Colour online) Snapshots of the isolines of $h_1(X, Y, \tau) - 1$; $M = -8$, $\Delta_X = 2$. (*a*) $\tau = 2\,050\,000$; (*b*) $\tau = 2\,050\,420$; (*c*) $\tau = 2\,050\,620$; (*d*) $\tau = 2\,051\,340$; (*e*) $\tau = 2\,051\,600$; (*f*) $\tau = 2\,051\,980$.

$s_{10}(\tau)$, $c_{10}(\tau)$ are small, a wave with two maxima and two minima is observed, due to the Fourier component s_{20} (see figure 35*c*).

The two-dimensional standing waves described above exist in a wide region of the parameters M and Δ_X.

5. Conclusions

The influence of a substrate temperature modulation on nonlinear Marangoni waves has been investigated. In the framework of a long-wave approach, the problem is reduced to a system of two coupled nonlinear equations for the surface deformations. Simulations have been carried out for several types of spatial temperature modulations. A number of physical phenomena have been revealed.

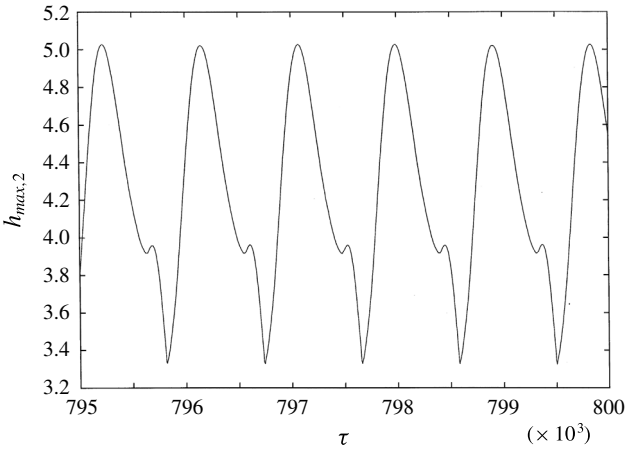

FIGURE 26. Oscillations of $h_{max,2}(\tau)$ for $M = -8$, $\Delta_X = 2$.

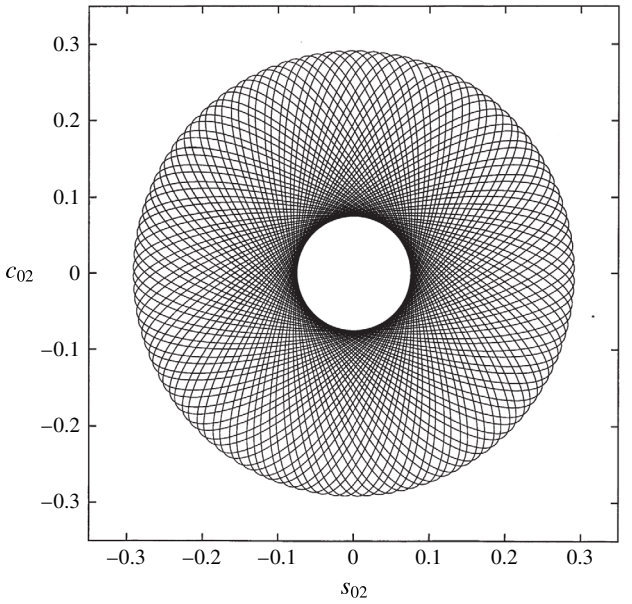

FIGURE 27. The phase trajectory in the plane s_{02}, c_{02}; $M = -8$, $\Delta_X = 2$.

On one hand, the non-uniformity of heating breaks the translational and rotational symmetries of the original problem. It tends to create a stationary flow with a symmetry corresponding to that of the modulation. This tendency competes with the intrinsic oscillatory instability of the system which generates wave motions. As a result of this competition, a number of nonlinear regimes are produced.

In the case of a small modulation amplitude, three-dimensional standing waves, similar to the alternating rolls of the original non-modulated problem, are developed. In the case of a one-dimensional modulation with a period equal to the length of the region, with the growth of the modulation parameter, this regime is replaced by two-dimensional standing waves, and then by a two-dimensional stationary flow. Wave

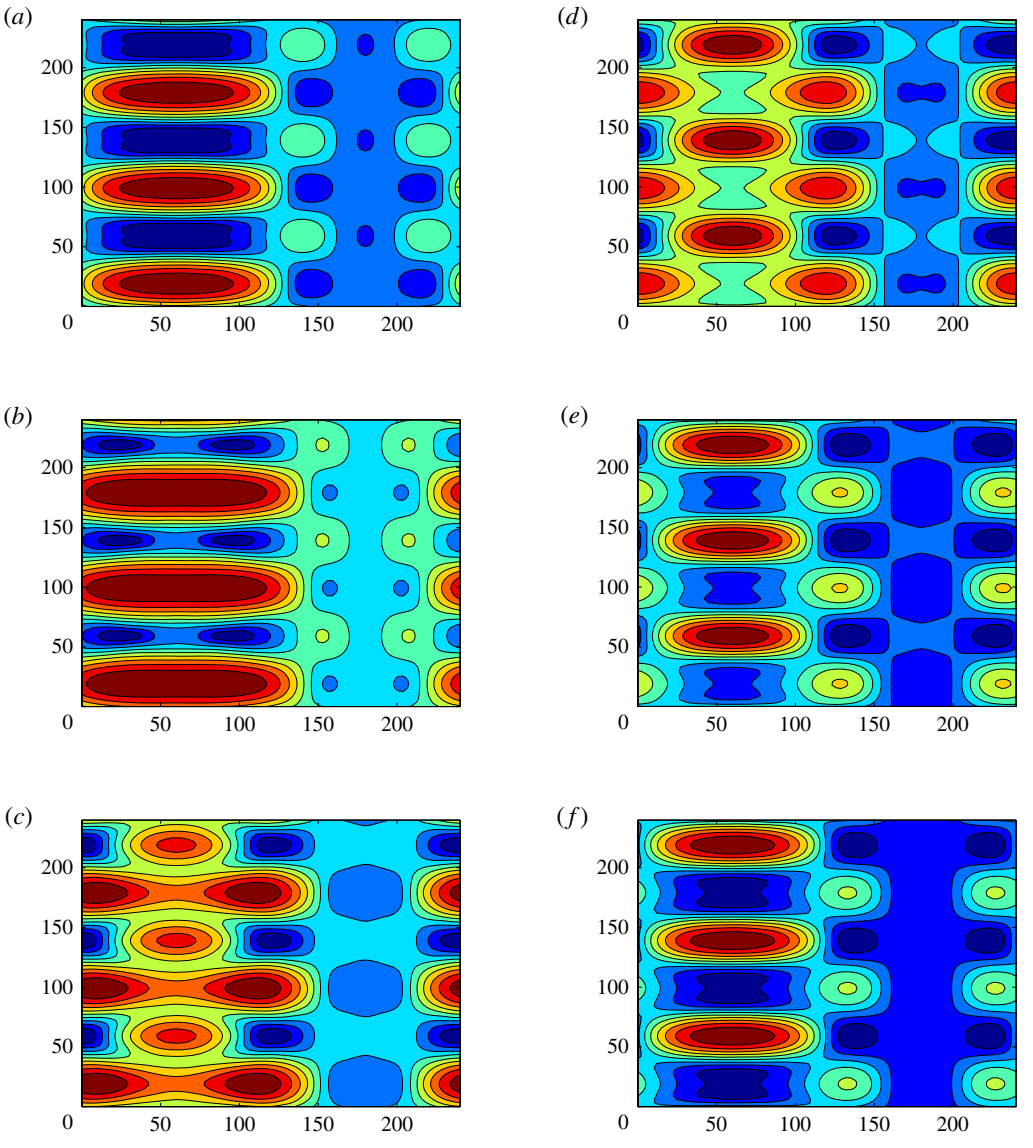

FIGURE 28. (Colour online) Snapshots of the isolines of $h_2(X, Y, \tau) - h$: (*a*) $\tau = 2\,050\,260$, (*b*) $\tau = 2\,050\,400$, (*c*) $\tau = 2\,050\,520$, (*d*) $\tau = 2\,050\,560$, (*e*) $\tau = 2\,050\,620$, (*f*) $\tau = 2\,050\,660$; $M = -6$, $\Delta_X = 3$.

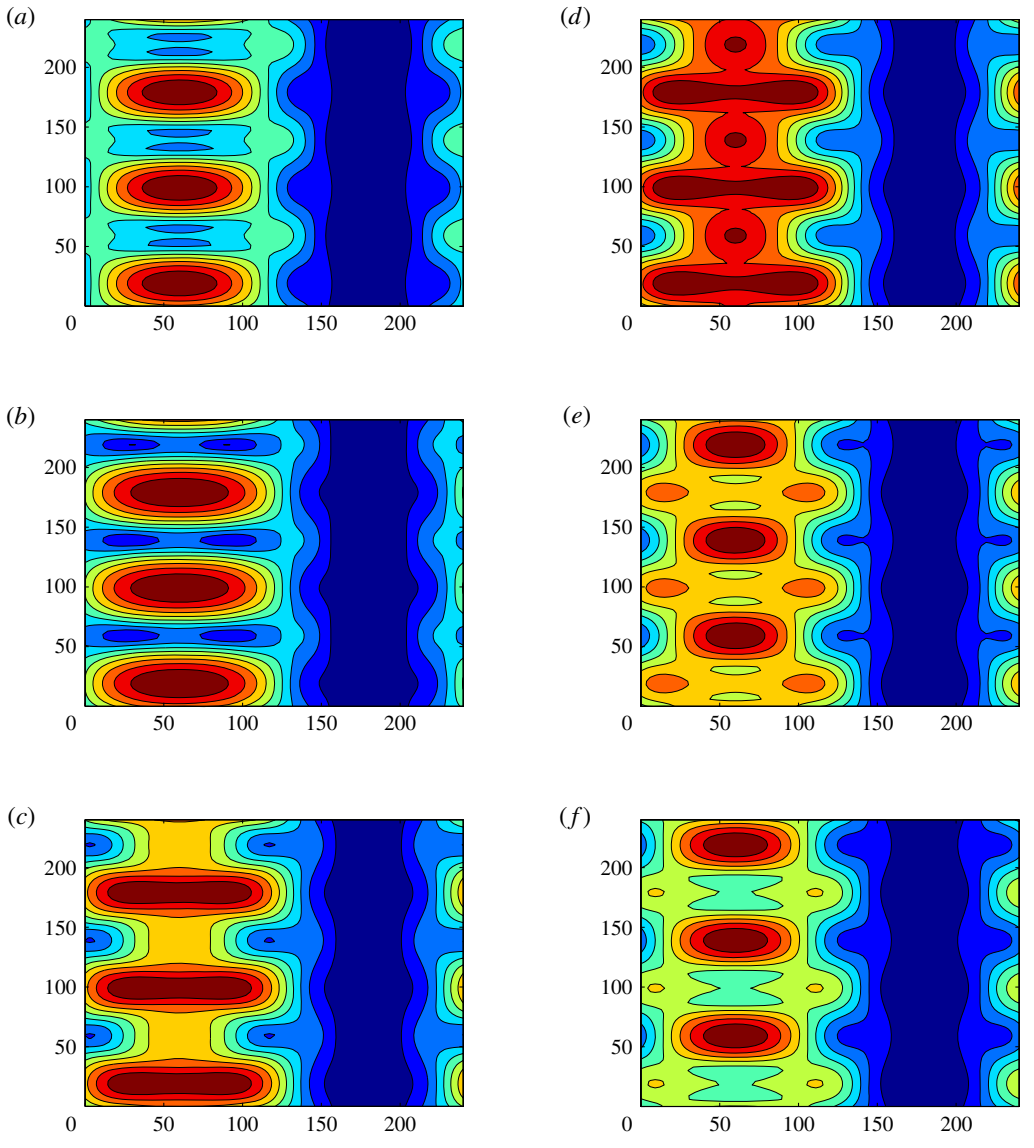

FIGURE 29. (Colour online) Snapshots of the isolines of $h_1(X, Y, \tau) - 1$: (*a*) $\tau = 2\,050\,260$, (*b*) $\tau = 2\,050\,400$, (*c*) $\tau = 2\,050\,520$, (*d*) $\tau = 2\,050\,560$, (*e*) $\tau = 2\,050\,620$, (*f*) $\tau = 2\,050\,660$; $M = -6$, $\Delta_X = 3$.

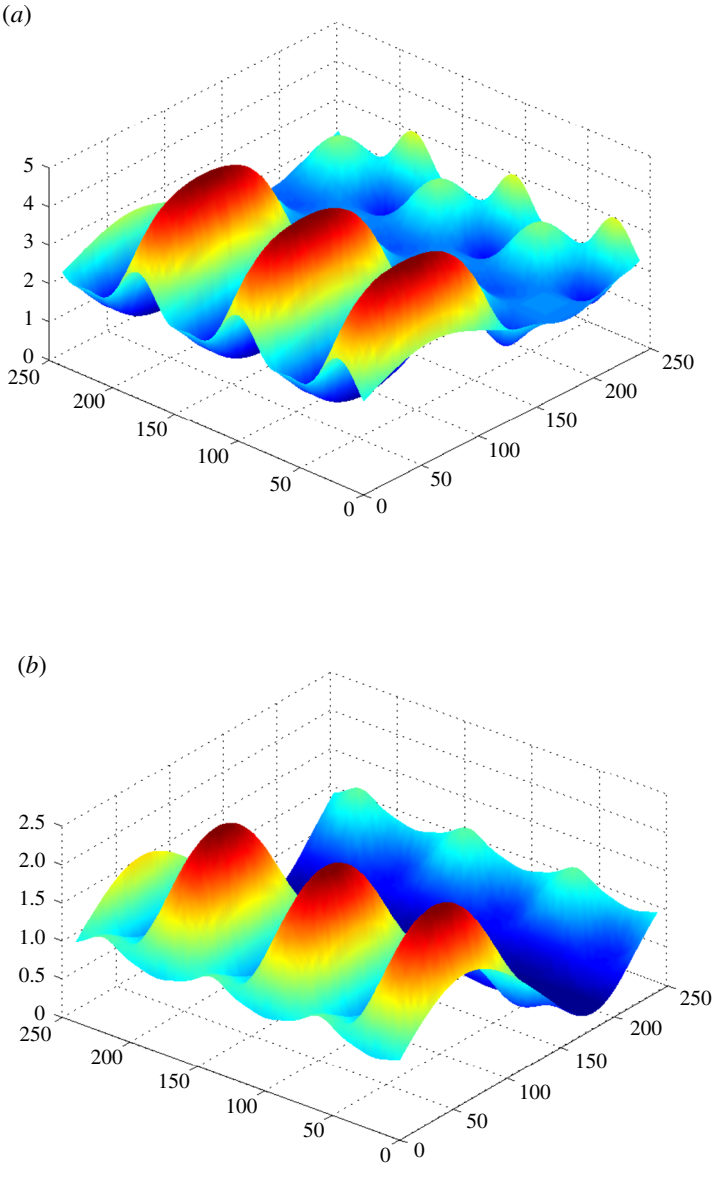

FIGURE 30. (Colour online) Shapes of (*a*) the upper surface $z = h_2(X, Y, \tau)$ and (*b*) the interface $z = h_1(X, Y, \tau)$; $M = -6$, $\Delta_X = 3$.

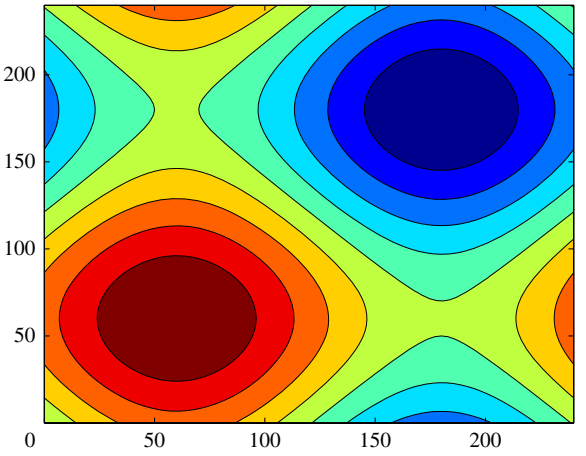

FIGURE 31. (Colour online) Snapshot of the isolines of $h_2(X, Y, \tau) - h$; $M = -2$, $\Delta_X = \Delta_Y = 0.5$.

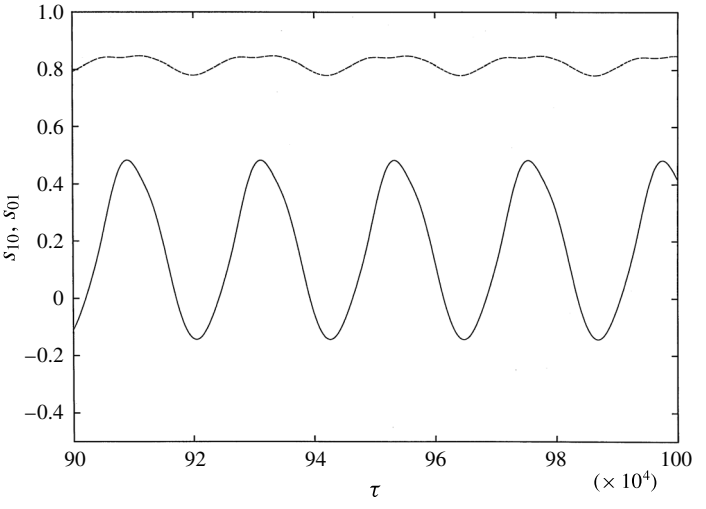

FIGURE 32. Oscillations of $s_{10}(\tau)$ (solid line) and s_{01} (dashed line) for $M = -2$, $\Delta_X = 0.2$, $\Delta_Y = 1$.

motions, travelling and standing, reappear with a further growth of the modulation amplitude. For sufficiently strong modulation and large values of the Marangoni number, structures with a shorter wavelength in the direction perpendicular to the substrate temperature gradient are observed. The general diagram of regimes has been constructed.

In the case of a two-dimensional modulation, the stationary flow is replaced by three-dimensional standing waves.

On the other hand, the imposed periodic perturbation creates an interaction between waves with different wavevectors. This can lead to the generation of a standing wave with a period that is two times larger than the period of the substrate temperature modulation ('spatial parametric resonance').

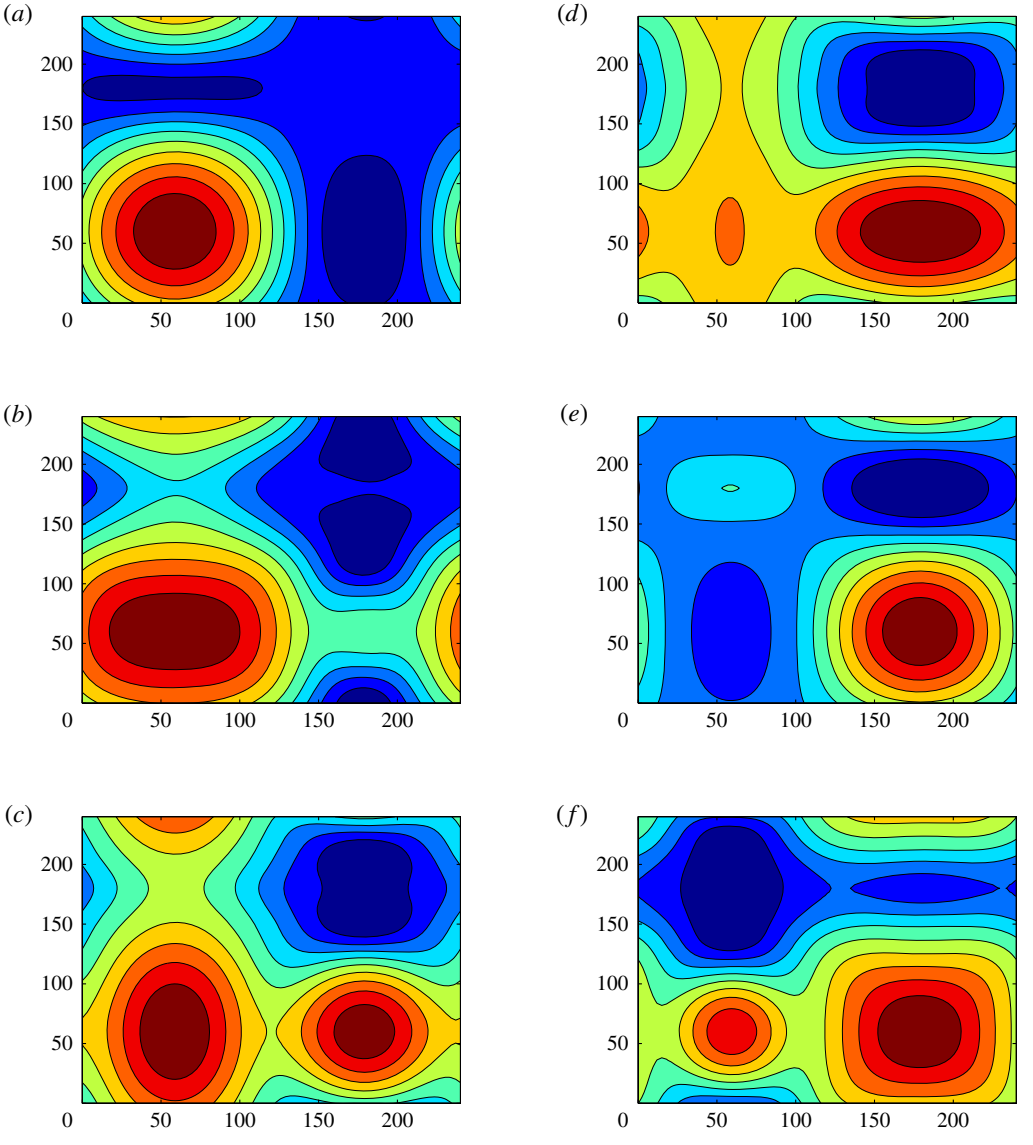

FIGURE 33. (Colour online) Snapshots of the isolines of $h_2(X, Y, \tau) - h$: (*a*) $\tau = 2\,004\,000$, (*b*) $\tau = 2\,004\,057$, (*c*) $\tau = 2\,004\,100$, (*d*) $\tau = 2\,004\,126$, (*e*) $\tau = 2\,004\,190$, (*f*) $\tau = 2\,004\,299$; $M = -2$, $\Delta_X = 0.2$, $\Delta_Y = 1$.

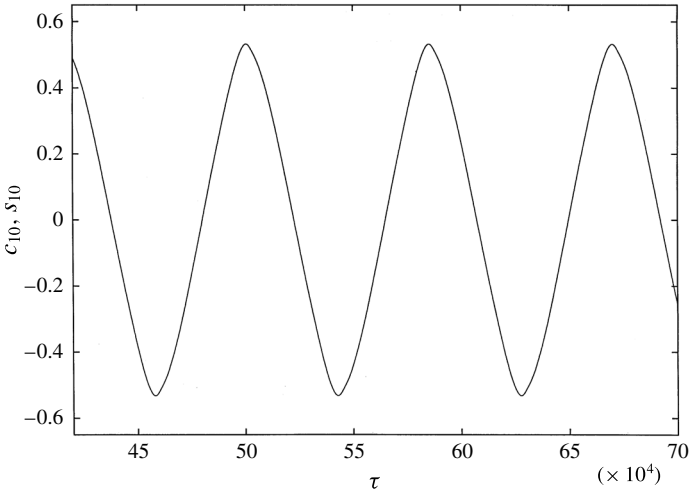

FIGURE 34. The temporal dependence of $s_{10}(\tau) = c_{10}(\tau)$ for $M = -2$, $\Delta_X = 0.75$.

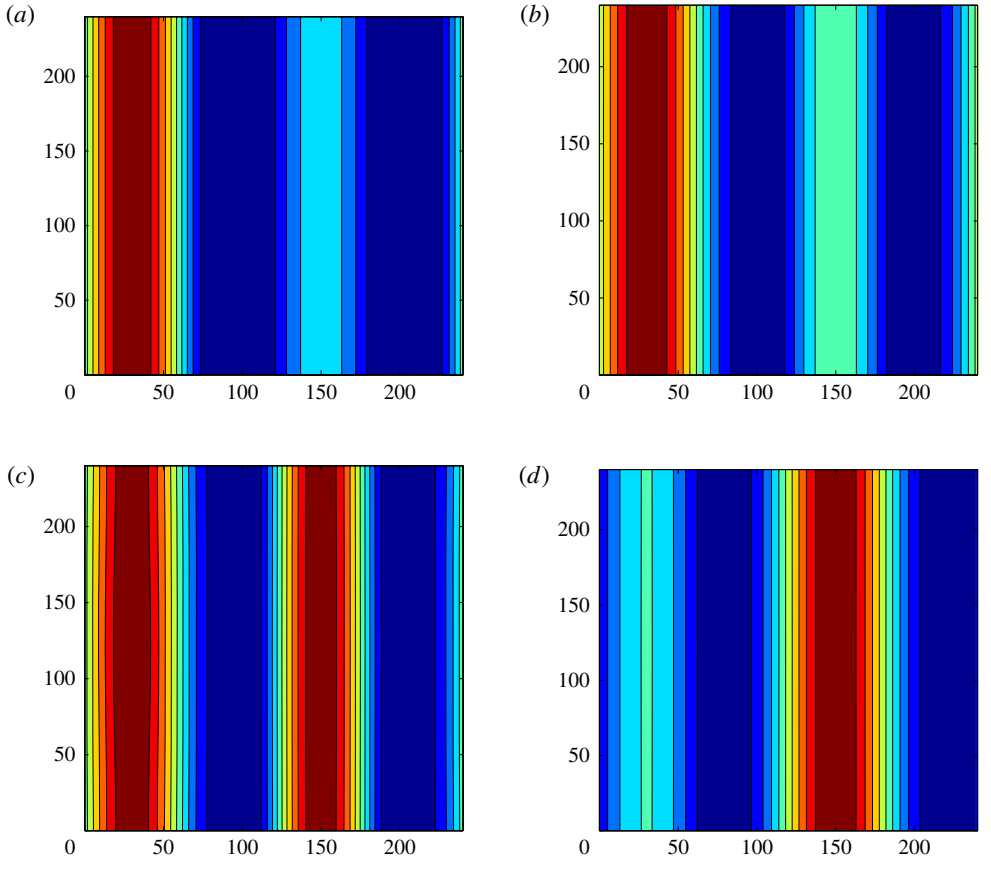

FIGURE 35. (Colour online) Snapshots of the isolines of $h_1(X, Y, \tau) - 1$: (*a*) $\tau = 492\,000$, (*b*) $\tau = 512\,330$, (*c*) $\tau = 522\,000$, (*d*) $\tau = 552\,000$; $M = -2$, $\Delta_X = 0.75$.

REFERENCES

ABARZHI, S. I., DESJARDINS, O., NEPOMNYASHCHY, A. & PITSCH, H. 2007 Influence of parametric forcing on the nonequilibrium dynamics of wave patterns. *Phys. Rev.* E **75**, 046208.

ARANSON, I. S. & KRAMER, L. 2002 The world of the complex Ginzburg–Landau equation. *Rev. Mod. Phys.* **74**, 99.

BANDYOPADHYAY, D., GULABANI, R. & SHARMA, A. 2005 Instability and dynamics of thin liquid bilayers. *Ind. Engng Chem. Res.* **44**, 1259.

COULLET, P., ELPHICK, C. & REPAUX, D. 1987 Nature of spatial chaos. *Phys. Rev. Lett.* **58**, 431.

CROSS, M. C. & HOHENBERG, P. C. 1993 Pattern formation outside of equilibrium. *Rev. Mod. Phys.* **65**, 851.

DAVIS, S. H. 1987 Thermocapillary instabilities. *Annu. Rev. Fluid Mech.* **19**, 403.

FISHER, L. S. & GOLOVIN, A. A. 2005 Nonlinear stability analysis of a two-layer thin liquid film: dewetting and autophobic behavior. *J. Colloid Interface Sci.* **291**, 515.

FREUND, G., PESCH, W. & ZIMMERMANN, W. 2011 Rayleigh–Bénard convection in the presence of spatial temperature modulations. *J. Fluid Mech.* 673, 318.

GÉORIS, PH., HENNENBERG, M., LEBON, G. & LEGROS, J. C. 1999 Investigation of thermocapillary convection in a three-liquid-layer system. *J. Fluid Mech.* **389**, 209.

HAIM, L., MAU, Y. & MERON, E. 2014 Spatial forcing of pattern-forming systems that lack inversion symmetry. *Phys. Rev.* E **90**, 022904.

HAMMELE, M. & ZIMMERMANN, W. 2006 Harmonic versus subharmonic patterns in a spatially forced oscillating chemical reaction. *Phys. Rev.* E **73**, 066211.

MALOMED, B. A. 1993 Ramp-induced wave-number selection for traveling waves. *Phys. Rev.* E **47**, R2257.

MANOR, R., HAGBERG, A. & MERON, E. 2008 Wave-number locking in spatially force pattern-forming systems. *Europhys. Lett.* **83**, 10005.

MAU, Y., HAIM, L., HAGBERG, A. & MERON, E. 2013 Competing resonances in spatial forced pattern-forming systems. *Phys. Rev.* E **88**, 032917.

MIKHAILOV, A. S. & SHOWALTER, K. 2006 Control of waves, patterns and turbulence in chemical systems. *Phys. Rep.* **425**, 79.

NEPOMNYASHCHY, A. A. 1988 Spatially modulated convective motions in a vertical layer with curved boundaries. *Z. Angew. Math. Mech.* **52**, 677.

NEPOMNYASHCHY, A. A. & ABARZHI, S. I. 2010 Monochromatic waves induced by large-scale parametric forcing. *Phys. Rev.* E **81**, 037202.

NEPOMNYASHCHY, A. A. & SHKLYAEV, S. 2016 Longwave oscillatory patterns in liquids: outside the world of the complex Ginzburg–Landau equation. *J. Phys. A: Math. Gen.* **49**, 053001.

NEPOMNYASHCHY, A. A. & SIMANOVSKII, I. B. 2006 Decomposition of a two-layer thin liquid film flowing under the action of Marangoni stresses. *Phys. Fluids* **18**, 112101.

NEPOMNYASHCHY, A. A. & SIMANOVSKII, I. B. 2007 Marangoni instability in ultrathin two-layer films. *Phys. Fluids* **19**, 122103.

NEPOMNYASHCHY, A. A. & SIMANOVSKII, I. B. 2012 Nonlinear Marangoni waves in a two-layer film in the presence of gravity. *Phys. Fluids* **24**, 032101.

ORON, A., DAVIS, S. H. & BANKOFF, S. G. 1997 Long-scale evolution of thin liquid films. *Rev. Mod. Phys.* **69**, 931.

PISMEN, L. M. 1987 Bifurcation of quasiperiodic and nonstationary patterns under external forcing. *Phys. Rev. Lett.* **59**, 2740.

POTOTSKY, A., BESTEHORN, M., MERKT, D. & THIELE, U. 2004 Alternative pathways of dewetting for a thin liquid two-layer film. *Phys. Rev.* E **70**, 025201.

POTOTSKY, A., BESTEHORN, M., MERKT, D. & THIELE, U. 2005 Morphology changes in the evolution of liquid two-layer films. *J. Chem. Phys.* **122**, 224711.

SCHÖLL, E. & SCHUSTER, H. G. (Eds) 2008 *Handbook of Chaos Control*, 2nd edn. Wiley-VCH, Weinheim.

SIMANOVSKII, I. B. & NEPOMNYASHCHY, A. A. 1993 *Convective Instabilities in Systems with Interface*. Gordon and Breach.

UTZNY, C., ZIMMERMANN, W. & BÄR, M. 2002 Resonant spatio-temporal forcing of oscillatory media. *Europhys. Lett.* **57**, 113.

VOZOVOI, L. P. & NEPOMNYASHCHY, A. A. 1974 Convection in the horizontal layer with the spatial modulation of the temperature on the boundaries. In *Hydrodynamics, pt.7* (ed. E. M. Zhukhovitskii), p. 107. Perm State Pedagogical Institute, (in Russian).

VOZOVOI, L. P. & NEPOMNYASHCHY, A. A. 1979 On the stability of spatially periodic convective flows in the vertical layer with curved boundaries. *Z. Angew. Math. Mech.* **43**, 1080.

WEISS, S., SEIDEN, G. & BODENSCHATZ, E. 2014 Resonance patterns in spatially forced Rayleigh–Bénard convection. *J. Fluid Mech.* **756**, 293.